Investigation of Wireless Power Transfer

Nicholas Rypkema
CSIRO ICT Centre

ICT 09/116

20 February 2009

Enquiries should be addressed to:
Dr Trevor S. Bird
email: trevor.bird@csiro.au; ph: (02) 9372 4289

Distribution list

Unlimited

Copyright and Disclaimer

Important Disclaimer

Contents

List of Figures

1. INTRODUCTION

The continuing reduction in size and power consumption of integrated circuits has led to an increasing interest in the research and development of wireless sensor networks. The vision for these networks is that they would be comprised of hundreds of small, low power and low cost wireless sensor nodes. These nodes would operate in a multi-hop fashion to replace long transmission distances, and would result in the creation of an intelligent environment, able to respond to its inhabitants and capable of monitoring various ambient conditions [1].

The wireless devices currently being designed and built to be used as nodes in such environments typically run on batteries, which results in a limited lifespan or operating time for these devices. As the number of nodes in a wireless sensor network increases, the cost in time and money to replace depleted batteries escalates to impractical levels, and may even be impossible when nodes are placed in inaccessible areas (e.g. nodes placed inside walls to monitor structural integrity). One possible solution would be to use a battery large enough to last the entire lifetime of the node. However, such a battery would dominate the overall size and cost of the system, and so is not an attractive option. An alternative method of powering the devices that make up wireless sensor networks is required [1].

Alternative power methods could include improved batteries or fuel cells, or they could include scavenging energy from the environment, such as photonic or solar, kinetic-flow, vibration, and thermal energies [2] [3]. Alternative power sources could also include methods of wirelessly distributing power to the nodes in the network, and wirelessly recharging batteries, such as radio-frequency (RF) energy transfer, which is the focus of this report.

This work reports on a research project that explores the issues surrounding wireless RF power transfer, in an attempt to determine its feasibility in wirelessly powering low-power (milliwatt) sensor devices. The report discusses the basic components of a wireless power transfer system, and attempts to investigate each component. Firstly, the power transfer possible between two antennas is investigated, with a theoretical model being derived, simulations undertaken, and experiments carried out. A circuit to rectify the transferred power is researched, and the important issues related to this circuit are studied. Finally, a basic wireless power transfer system is simulated to get an idea about the behaviour of such a system. Unfortunately, due to lack of time, a number of components in the system and issues could not be investigated, and recommendations for future research and work are given at the end of this report.

The hope is that the findings in this report will provide a sound basis for further research in this area.

2. BACKGROUND

Shown below in Figure 2.1 is a block diagram of a basic wireless power transfer system. In this work it will be assumed that at the transmitter end electrical energy can be converted to RF power and relayed to an antenna with high efficiency and the main problem to be solved is at the receiver end of the system. The antennas transfer RF power from the transmitter to a receiving antenna, where it is rectified and stored by the rectifier/voltage multiplier circuit to provide power to the load. The matching network is needed to reduce any loss of power due to impedance mismatch between the receiving antenna and the rest of the system. The power management circuit determines how power is applied to the load, depending on the requirements of the entire system as well as the load. This paper focuses mainly on the antennas, and to a lesser extent, the rectifier/voltage multiplier and impedance matching circuit. Because there is a lot of theory related to specific parts of the system, the theory will be detailed in individual sections of the report instead of in this section.

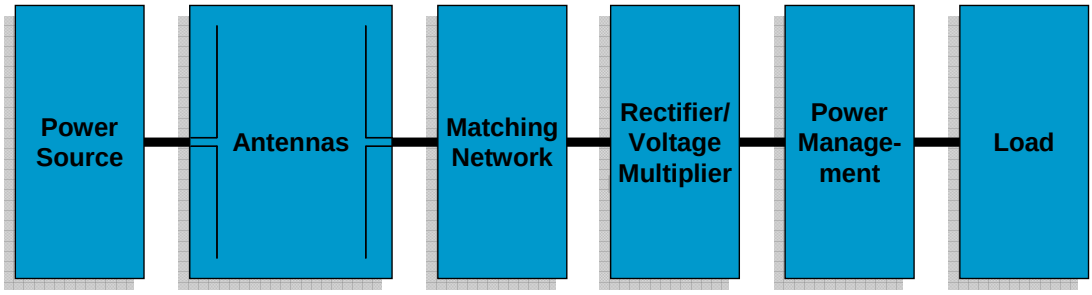

Figure 2.1: Block diagram of a basic wireless power transfer system.

At this time there are few published research papers on the investigation of wireless power transfer for powering low-power sensor devices or recharging batteries [4], [5], [6], [7]. This investigation was motivated by the Master's thesis by Daniel Harrist, "Wireless Battery Recharging System Using Radio Frequency Energy Harvesting" [8]. Unfortunately this thesis is sparse on detail, and provided little information on which to base an investigation of wireless power transfer. A short review on the flaws of the Harrist thesis is provided in Appendix A. However, there are quite a few published papers which have information on the issues surrounding wireless power transfer, which are about passive RFID devices, such as [9], [10] and [11]. The issues faced for both this wireless power transfer investigation, as well as power transfer in RFID tags are basically identical, with the difference being that RFID tags can operate at considerably lower power levels than what is wanted for this wireless power transfer system. RFID papers were a good source of information used in this investigation, and provide general background theory relating to wireless power transfer.

3. ANTENNAS

The first part of the project was to determine the power transfer possible between a transmitting and receiving antenna. A circuit model of two arrays of linear antennas was investigated, where linear antennas were modelled in Matlab, simulated, as well as experimentally investigated.

3.1 Modelling

To understand the transfer of power using antennas, and to estimate the relationship of power transfer versus distance between antennas, a transmitting and receiving antenna system must be modelled. Traditionally, in RFID design, various forms of the Friis transmission equation are used to calculate the PTE [12] [13], or Power Transfer Efficiency (the ratio of the power received by the receiving antenna to the power input into the transmitting antenna) of the antenna system. However, this equation is valid only for far-field situations. In order to allow validity in both near and far-field situations, a different method was used in this project to calculate the PTE. This model and all its theory is based on the Balanis book, "Antenna Theory" [14].

3.1.1 Mutual Coupling

In order for the antenna system model to be valid in the near-field, it is important to consider the effects of mutual coupling. When two antennas are near each other, the impedance, current distribution, radiated field, and other properties of one antenna are affected by the presence of the other, in an effect called mutual coupling. The input impedance of an antenna in the presence of another depends on its self-impedance (input impedance in the absence if any other elements) and the mutual impedance between it and all other elements. Thus, the interaction and mutual effects between the elements of the antenna system must be taken into account when calculating the power transfer between the transmitting and receiving antennas.

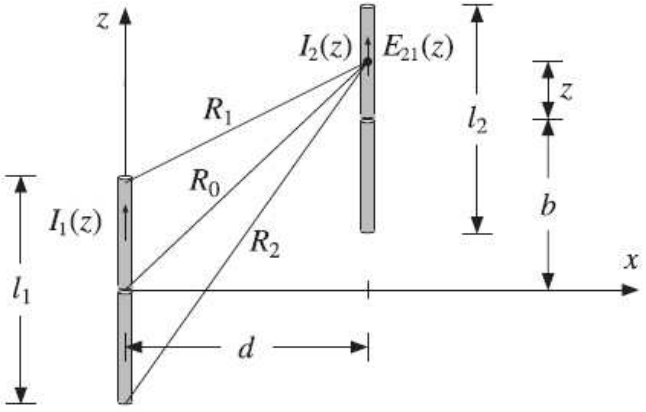

Figure 3.1: Parallel linear dipoles.

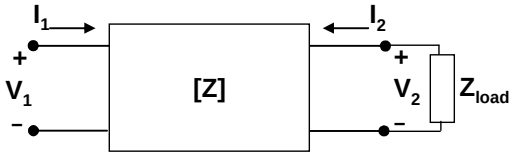

Figure 3.2: Two-port network with load impedance

To simplify the modelling of the receiving and transmitting antennas, the two antennas were initially chosen to be thin-wire, linear dipoles. Looking at the Figure 3.1 above, this system can be represented by a two-port (four-terminal) network (Figure 3.2), and by the following voltage-current relations:

$$\begin{aligned} V_1 &= Z_{11} I_1 + Z_{12} I_2 \\ V_2 &= Z_{21} I_1 + Z_{22} I_2 \end{aligned} \tag{1}$$

Where

$$Z_{11} = V_1 / I_1 \Big|_{I_2=0} \tag{2}$$

is the input impedance of antenna 1 (port 1) with antenna 2 (port 2) open circuited,

$$Z_{12} = V_1 / I_2 \Big|_{I_1=0} \tag{3}$$

is the mutual impedance of antenna 1 (at port 1) due to a current on antenna 2 (at port 2),

$$Z_{21} = V_2 / I_1 \Big|_{I_2=0} \tag{4}$$

is the mutual impedance of antenna 2 (at port 2) due to a current on antenna 1 (at port 1),

$$Z_{22} = V_2 / I_2 \Big|_{I_1=0} \tag{5}$$

is the input impedance of antenna 2 (port 2) with antenna 1 (port 1) open circuited.

The impedances Z_{11} and Z_{22} are the self-impedances of the two antennas and are approximately equal to the input impedances of the isolated antennas (i.e. when the other antenna is absent).

Referring to Figure 3.1, the induced open-circuit voltage in antenna 2, due to the radiation from antenna 1, is given by (the integration of the electric field and current distribution along the antenna):

$$V_{21} = -\frac{1}{I_2(0)} \int_{-L2/2}^{L2/2} E_{21}(z) I_2(z) dz \tag{6}$$

Where $I_2(0)$ and $I_2(z)$ are the input current and current distribution on antenna 2 when it is transmitting, and $E_{21}(z)$ is the E-field component radiated by antenna 1, which is parallel to antenna 2. Therefore the mutual impedance, Z_{21}, is expressed as:

$$Z_{21} = \frac{V_{21}}{I_1(0)} = -\frac{1}{I_1(0)I_2(0)}\int_{-L2/2}^{L2/2} E_{21}(z)I_2(z)dz \qquad (7)$$

In order to evaluate this integral, expressions for the incident E-field and current distributions must be found. To obtain accurate expressions, the Integral Equation-Moment Method can be used, but this requires lengthy formulation and computer programming. To simplify the analysis, the Induced EMF Method is used, which uses the following current distribution on a linear wire of length L: [Balanis]

$$I(z) = I_{\max}\sin\left[k\left(\frac{L}{2} - |z|\right)\right] \qquad (8)$$

The radiated electric field in the z-direction due to this current is (with reference to Figure 3.1)

$$\mathrm{E_z(z)} = \frac{-\mathrm{j}\eta \mathrm{I_{max}}}{4\pi}\left[\frac{\mathrm{e^{-jkR_1}}}{\mathrm{R_1}} + \frac{\mathrm{e^{-jkR_2}}}{\mathrm{R_2}} - 2\cos\left(\mathrm{k}\frac{\mathrm{L}}{2}\right)\frac{\mathrm{e^{-jkR_0}}}{\mathrm{R_0}}\right] \qquad (9)$$

with

$$\mathrm{R_0} = \sqrt{\mathrm{d}^2 + (\mathrm{z}+\mathrm{b})^2}$$
$$\mathrm{R_1} = \sqrt{\mathrm{d}^2 + (\mathrm{z}+\mathrm{b}-\mathrm{L_1}/2)^2}$$
$$\mathrm{R_2} = \sqrt{\mathrm{d}^2 + (\mathrm{z}+\mathrm{b}+\mathrm{L_1}/2)^2}$$

Note that the current equation makes the assumption that the current distribution along the dipole is sinusoidal. For a full explanation on how these expressions are derived, see any electromagnetics textbook on near fields of dipoles (e.g. [14]).

By inserting these equations into the expression for mutual impedance, and after rearranging some constants, the final equation for mutual impedance is

$$Z_{21} = \frac{j\eta}{4\pi\sin\left(\frac{kL_1}{2}\right)\sin\left(\frac{kL_2}{2}\right)}\int_{-L_2/2}^{L_2/2}\left[\frac{e^{-jkR_1}}{R_1} + \frac{e^{-jkR_2}}{R_2} - 2\cos\left(k\frac{L_1}{2}\right)\frac{e^{-jkR_0}}{R_0}\right]\sin\left[k\left(\frac{L_2}{2} - |z|\right)\right]dz \qquad (10)$$

This is the mutual impedance referred to the input terminals of the antennas. It should be noted that this expression has limitations. If either of the antennas have a length that is a multiple of λ, then either of the denominator factors $\sin(kL_1/2)$ or $\sin(kL_2/2)$ will vanish, resulting in an infinite mutual impedance. This limitation is due to the assumed sinusoidal current distribution

of the antennas. Since the input current of an actual antenna is never zero, this equation is valid only for dipole antennas close to half-wavelength long, where current becomes zero at the end of the dipoles, and where the sinusoidal approximation is good. Thus, to allow accurate modelling of dipoles longer than half wavelength, a more accurate expression for the current distributions of the dipoles is needed, which was beyond the scope of this project.

The self impedances Z_{11} and Z_{22} can also be calculated using the same equation as Z_{21} and Z_{12}. For example, by evaluating the near-field on the surface of the single antenna (i.e. letting d = a, where a is the antenna radius), and by setting b = 0 and $L_2/2 = L_1/2$, the following is obtained

$$Z_{11} = \frac{j\eta}{4\pi \sin^2\left(\frac{kL_1}{2}\right)} \int_{-L_1/2}^{L_1/2} \left[\frac{e^{-jkR_1}}{R_1} + \frac{e^{-jkR_2}}{R_2} - 2\cos\left(k\frac{L_1}{2}\right)\frac{e^{-jkR_0}}{R_0} \right] \sin\left[k\left(\frac{L_1}{2} - |z|\right)\right] dz \tag{11}$$

Similar expressions for both Z_{22} and Z_{12} can be found. This general impedance equation is evaluated numerically using the Matlab file mutual_imped.m (see Appendix D).

3.1.2 Adding Parasitic Elements

Once the impedance equation was determined, the evaluation of this equation allowed the modelling of the transmitting and receiving antennas as a two-port network. Note that it is also possible to introduce additional parasitic elements into the system, while maintaining this two-port network model. For example, adding a third parasitic (i.e. not driven by a voltage) thin-wire element would mean that the additional impedances Z_{13}, Z_{23}, Z_{31}, Z_{32} and Z_{33} must be calculated. The voltage-current relations of this system would then become:

$$\begin{aligned} V_1 &= Z_{11}I_1 + Z_{12}I_2 + Z_{13}I_3 \\ V_2 &= Z_{21}I_1 + Z_{22}I_2 + Z_{23}I_3 \\ 0 &= Z_{31}I_1 + Z_{32}I_2 + Z_{33}I_3 \end{aligned} \tag{12}$$

Since the last equation in (12) is for the parasitic element, it can be solved to get an expression for I_3 in terms of I_1 and I_2, which can then be substituted back into V_1 and V_2 to maintain the two-port model (i.e. V_1 and V_2 are dependant only on I_1 and I_2). An arbitrary number of additional parasitic elements can be introduced and the system can always be reduced back into a two-port network model. This process was done with two additional parasitic elements added to the dipole system, to model an antenna system with two-element Yagi antennas as the transmitting and receiving antennas (Figure 3.3). The system voltage-current relations are then:

$$\begin{aligned} V_1 &= Z_{11}I_1 + Z_{12}I_2 + Z_{13}I_3 + Z_{14}I_4 \\ V_2 &= Z_{21}I_1 + Z_{22}I_2 + Z_{23}I_3 + Z_{24}I_4 \\ 0 &= Z_{31}I_1 + Z_{32}I_2 + Z_{33}I_3 + Z_{34}I_4 \\ 0 &= Z_{41}I_1 + Z_{42}I_2 + Z_{43}I_3 + Z_{44}I_4 \end{aligned} \tag{13}$$

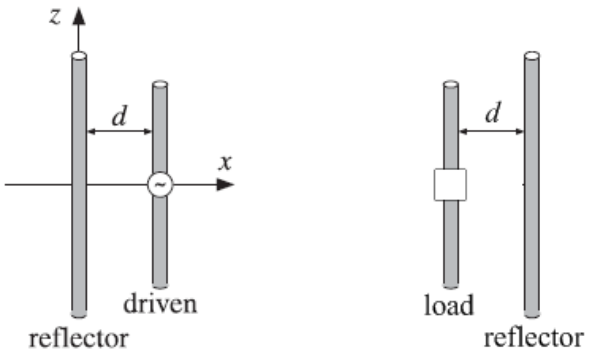

Figure 3.3: Parallel linear two-element Yagi antennas.

Solving the last two equations of (13) simultaneously results in:

$$\begin{aligned} Z_{11new} &= Z_{11} + Z_{13}\frac{e}{d} + Z_{14}\frac{b}{a} \\ Z_{12new} &= Z_{12} + Z_{13}\frac{f}{d} + Z_{14}\frac{c}{a} \\ Z_{21new} &= Z_{21} + Z_{23}\frac{e}{d} + Z_{24}\frac{b}{a} \\ Z_{22new} &= Z_{22} + Z_{23}\frac{f}{d} + Z_{24}\frac{c}{a} \end{aligned} \tag{14}$$

where,

$$a = Z_{44} - \frac{Z_{43}Z_{34}}{Z_{33}} \qquad d = Z_{33} - \frac{Z_{34}Z_{43}}{Z_{44}}$$

$$b = \frac{Z_{43}Z_{31}}{Z_{33}} - Z_{41} \qquad e = \frac{Z_{34}Z_{41}}{Z_{44}} - Z_{31}$$

$$c = \frac{Z_{43}Z_{32}}{Z_{33}} - Z_{42} \qquad f = \frac{Z_{34}Z_{41}}{Z_{44}} - Z_{32}$$

The system is now a two-port network, with the currents and voltages of the two Yagi antennas related by Z_{11new}, Z_{12new}, Z_{21new} and Z_{22new}. For a full derivation of the above equations, see Appendix B. It is interesting to note that if and only if $Z_{xy} = Z_{yx}$, then $Z_{12new} = Z_{21new}$, meaning that reciprocity still holds with the addition of parasitic elements (see Appendix B for this derivation). These two element Yagi antennas are used for both the receiving and transmitting antennas in the wireless power transfer system (Figure 2.1), for all further work in this project, due to its greater gain and directivity compared to dipoles.

3.1.3 Two-Port Network Model

As the antennas are modelled as a two-port network, standard two-port network theory can be used to derive expressions for the PTE, the induced current, and the induced voltage at the load of the receiving antenna. The derivation of these equations (referring to Figure 3.2) is described below.

To begin, the input impedance of antenna 1 (the transmitting antenna at port 1) is given by

$$Z_{in} = Z_{11} - \frac{Z_{12}Z_{21}}{Z_{22} + Z_{load}} \tag{15}$$

The output power at load of receiving antenna [port 2] is

$$P_{out} = 0.5\,\mathrm{Re}\{Z_{load}\}|I_2|^2 \tag{16}$$

While input power at transmitting antenna [port 1] is

$$P_{in} = 0.5\,\mathrm{Re}\{Z_{in}\}|I_1|^2 . \tag{17}$$

Now since

$$\left.\begin{aligned} \mathrm{V}_2 &= \mathrm{Z}_{21}\mathrm{I}_1 + \mathrm{Z}_{22}\mathrm{I}_2 \\ \mathrm{V}_2 &= -\mathrm{I}_2\mathrm{Z}_{\mathrm{load}} \end{aligned}\right\}$$

then

$$\mathrm{I}_2 = -\mathrm{I}_1\left(\frac{\mathrm{Z}_{21}}{\mathrm{Z}_{22} + \mathrm{Z}_{\mathrm{load}}}\right) \tag{18}$$

Substituting (18) into (16) gives:

$$P_{out} = 0.5\,\mathrm{Re}\{Z_{load}\}\left|\frac{Z_{21}}{Z_{22} + Z_{load}}\right|^2 |I_1|^2 \tag{19}$$

Therefore:

$$PTE = \frac{P_{out}}{P_{in}} = \frac{\mathrm{Re}\{Z_{load}\}}{\mathrm{Re}\{Z_{in}\}}\left|\frac{Z_{21}}{Z_{22} + Z_{load}}\right|^2 \tag{20}$$

Equation (20) for Power Transfer Efficiency (PTE) is seen to be dependant only on the impedances, Z_{11}, Z_{12}, Z_{21}, Z_{22} and Z_{load}. The current and voltage magnitudes at the load of the receiving antenna can also be found as:

$$|I_2| = \sqrt{P_{out}/\mathrm{Re}\{Z_{load}\}}$$
$$|V_2| = |I_2 Z_{load}|$$

The equation for PTE is most important, as it allows the calculation of power transfer versus distance between the transmitting and receiving antennas for a chosen load impedance, through the calculation of the mutual and self-impedances of the two antennas. This two-port network antenna model therefore provides a description of the behaviour of the transmitting and receiving antennas. The impedance calculation of the antenna system (with the antennas both being two-element Yagis), as well as the PTE calculation, at a certain distance, is evaluated

using the Matlab function power_transfer_yagis.m. The Matlab script power_transfer_yagis_graphing.m calculates the PTE using power_transfer_yagis.m over a range of distances and plots out the result of PTE versus distance. For information on both programs please refer to Appendix D.

It is interesting to compare this two-port network model with the Friis transmission equation. A comparison is shown below (Figure 3.4) for a half-wavelength dipole for both the transmitting and receiving antennas. It can be seen that the two-port model approaches the Friis model at farther antenna separation distances, but is also valid at closer distance (unlike the Friis model, which approaches infinity). Note that the load in the two-port model is matched, and the antennas are in a side-by-side arrangement (i.e. there is no offset), to allow comparison with the Friis model. The Friis approximation is clearly quite accurate at a distance greater than about two wavelengths.

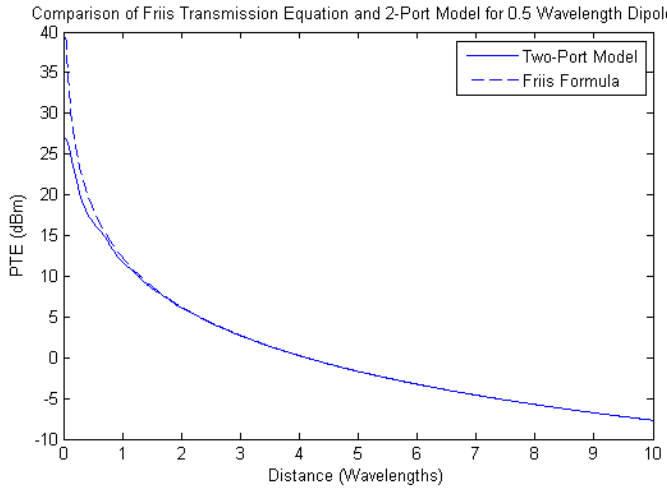

Figure 3.4: Comparison of power transfer using Friis and two-port model.

3.1.4 Maximising Power Transfer Efficiency

The expression for Power Transfer Efficiency can be maximized in order to determine the conditions under which maximum power transfer occurs. Given that all the antenna impedances are known, it is obvious that when the two-port model for the antennas is known the PTE equation is dependant only on the value of the load impedance. Thus, it is a function of two variables, the resistance and reactance of the load. The complex impedance value at which maximum power transfer occurs can therefore be found by calculating the gradient of the PTE equation, and solving the gradient for zero, as is done to find the maximum of any two variable function. Note that although the impedance is complex, since the PTE returns a real value, it is a function of two real variables, and not of one real and one imaginary variable. The gradient of the PTE is solved for zero, as shown below (a full derivation is provided in Appendix C).

$$\nabla PTE(Z_{load}) = \left(\frac{\partial PTE}{\partial R_{load}}, \frac{\partial PTE}{\partial X_{load}} \right) = 0$$
$$\frac{\partial PTE}{\partial R_{load}} = 0; \frac{\partial PTE}{\partial X_{load}} = 0 \qquad (21)$$

$$R_{load} = \sqrt[+]{R_{22}{}^2 - R_{22}(R_{12}R_{21} - X_{12}X_{21})/R_{11} - (R_{12}X_{21} + R_{21}X_{12})^2/(4R_{11}{}^2)}$$
$$X_{load} = -X_{22} + (R_{12}X_{21} + R_{21}X_{12})/2R_{11} \quad (22)$$

It is of interest when looking at the result of this calculation that as the antenna separation approaches infinity, the elements with subscripts 12 and 21 approach zero. If this occurs, it is apparent that the result reduces to $R_{load} = R_{22}$ and $X_{load} = -X_{22}$. Therefore, at large distances between the antennas, the maximum power transfer theorem is satisfied, that is, maximum power is transferred when the load impedance is the complex conjugate of the receiving antenna self-impedance (Z_{22}). Intuitively, it is expected that the theorem is satisfied at all distances, but this has not been studied in depth during this project. A graph of the load impedance for maximum power transfer (referred to as a matched condition), versus distance between the antennas, can be generated using Matlab file max_power_transfer_conditions.m. For example, the load impedance for maximum power transfer for two side-by-side half-wavelength dipoles over a range of separation distances is shown in Figure 3.6. It can be seen that the value for the load impedance to achieve maximum transfer varies with separation, due to mutual coupling. Also, as expected, the load value approaches about 73-42j as antenna separation increases, which is the conjugate of the impedance of a half-wavelength dipole.

It is interesting to note, that if the load is continuously modified to be matched to the receiving antenna as the antenna separation changes, the graph of Figure 3.5 is obtained. This is a graph of maximum coupling, and represents the absolute best case scenario for antenna power transfer. Obviously, the load cannot change in real-life, and so it is usually chosen to obtain matching at the maximum separation distance required. It should be noted that this calculation of maximum coupling achieves exactly identical results as the calculation of maximum coupling using the Linville method [14] [15].

To conclude, the transmitting and receiving antennas of the power transfer system have both been chosen to be a two-element Yagi antenna. The antenna system has been modelled as a two-port network, with their currents and voltages related by the self and mutual impedances of the antennas. The induced current and voltage, as well as the Power Transfer Efficiency, are calculated using standard two-port network theory. The output of this model will be compared to the output from an accurate antenna simulation program, as described later in this report.

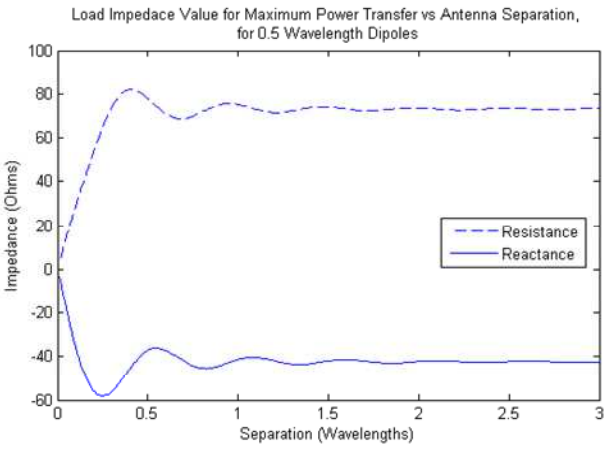

Figure 3.6: Load impedance value for maximum PTE.

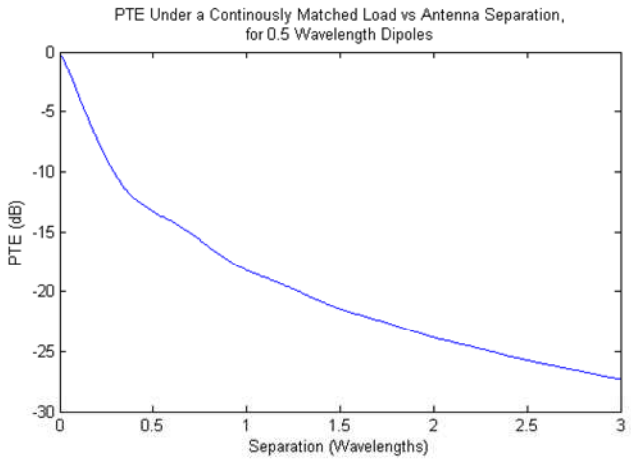

Figure 3.5: PTE with a continuously matched load.

3.2 Simulation

Simulation of the transmitting and receiving antennas was performed using a NEC2 integral equation moment-method program, called 4nec2 [16]. In order to test the validity of the two-port network model, simulation results were needed for comparison purposes. This program allows the modelling of antennas made of linear elements. A sample screenshot of the program is shown in Figure 3.7 below, where both the transmitting and receiving antennas are two-element Yagi antennas.

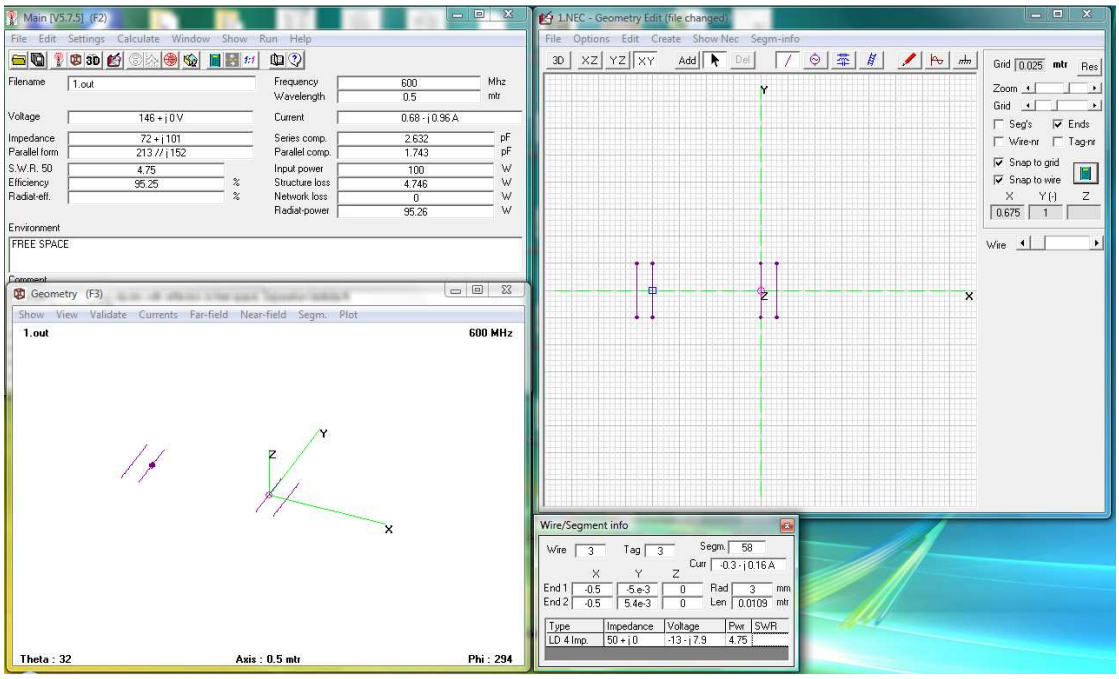

Figure 3.7: Screenshot of the 4nec2 simulation program.

The antennas are simply drawn up as lines in the program, a voltage source is placed in the centre of the transmitting antenna, and a lumped impedance is placed in the centre of the receiving antenna. When the program is run, the load is selected to see the power, voltage and current at the load. The power at the load was simulated for various antenna separation distances, for comparison with the two-port model. These simulations were also repeated for various load impedances, as well as a variety of antenna configurations (i.e. different antenna lengths and reflector element distances).

In order to determine the optimum two element Yagi antenna configuration (i.e. optimum element length and distance between the Yagi driven/load and reflector elements), extensive simulations with various configurations was undertaken. This process was done by firstly choosing the distance between the two antennas (between the driven element of the transmitting and load element of the receiving) to be a constant 1 wavelength apart. The length of all elements for both antennas was then selected. The distance between the driven or load element (depending if the antenna is receiving or transmitting) and the reflector element (the length d in Figure 3.3) was then selected, and this isolated Yagi antenna configuration was simulated to determine its impedance. The load of the receiving antenna was then set to the conjugate of this

impedance, and the two elements were then simulated to determine the power transfer for that specific configuration. This process was then repeated for differing driven/load element and reflector element separation lengths. Finally, the entire process was repeated for increasing antenna lengths. These extensive simulations revealed that for antenna lengths not equal to 0.5λ, 1.5 λ, 2.5λ etc. the power transfer is a decaying sinusoid as the reflector separation increases, and the power transfer obviously approaches that of two dipoles as the reflector separation increases. As well as this, it was found that maximum power transfer occurs for half wavelength Yagis, with as small as physically possible reflector separation. A few results of this process are shown below.

Figure 3.8: A few results from extensive simulations, to determine the optimum Yagi length and reflector spacing, for maximum PTE

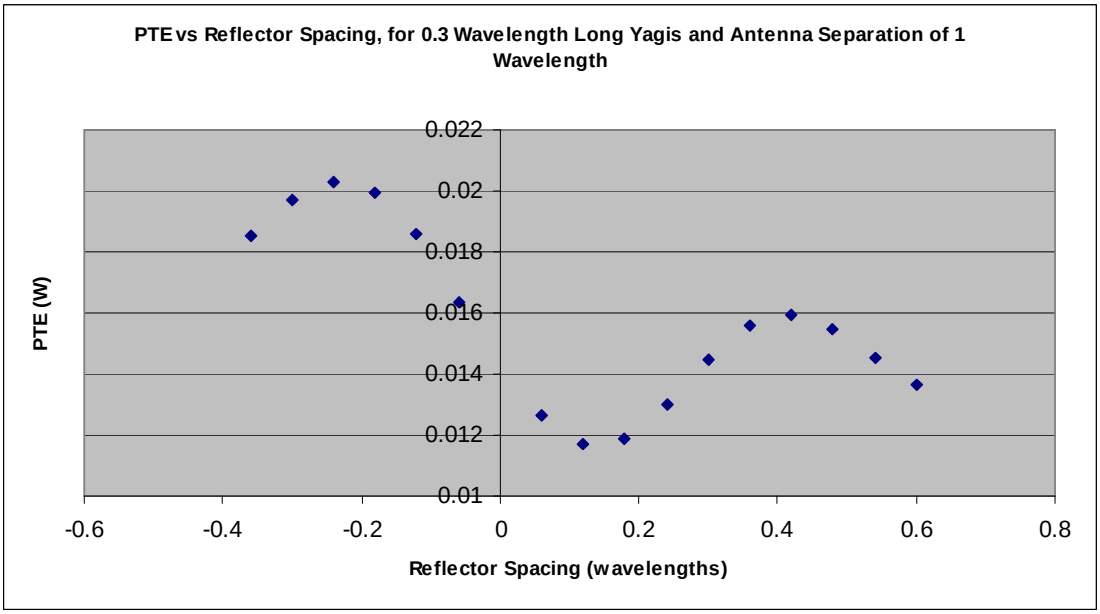

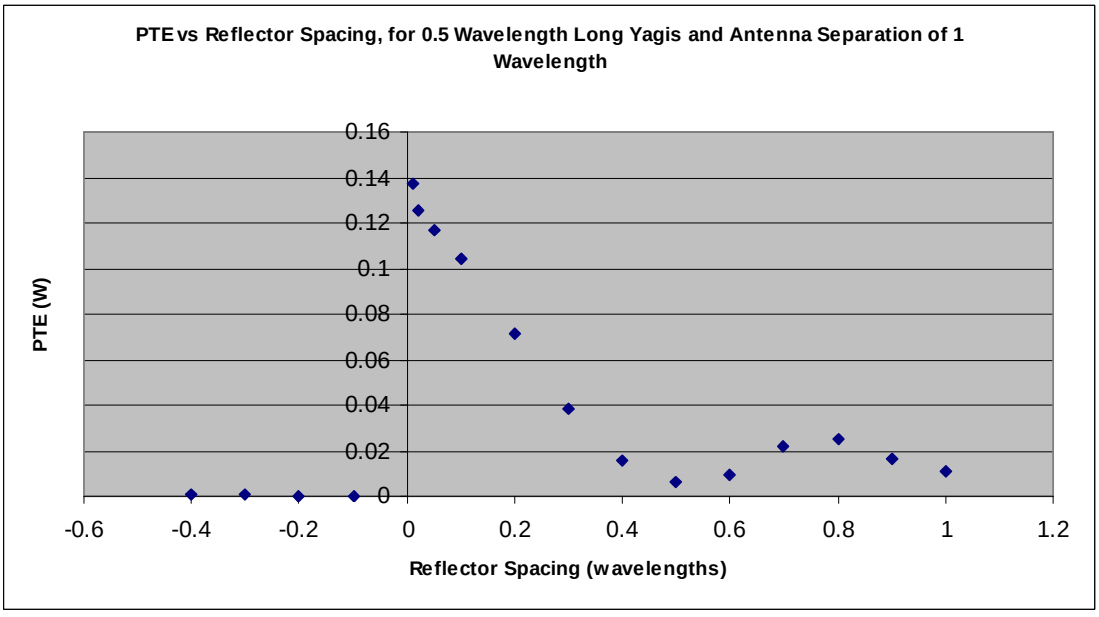

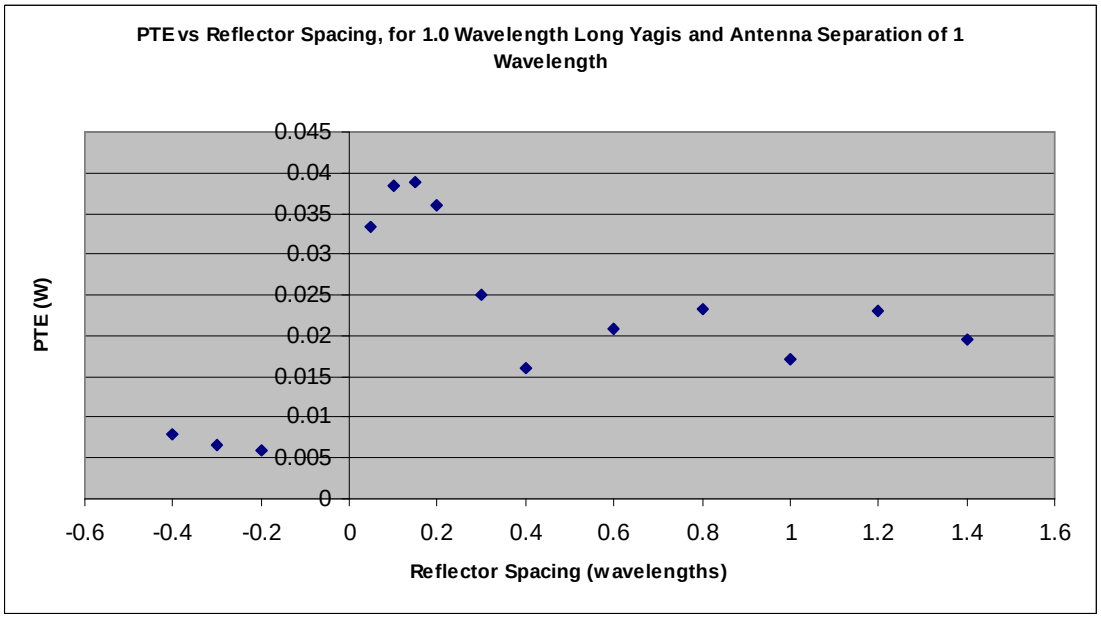

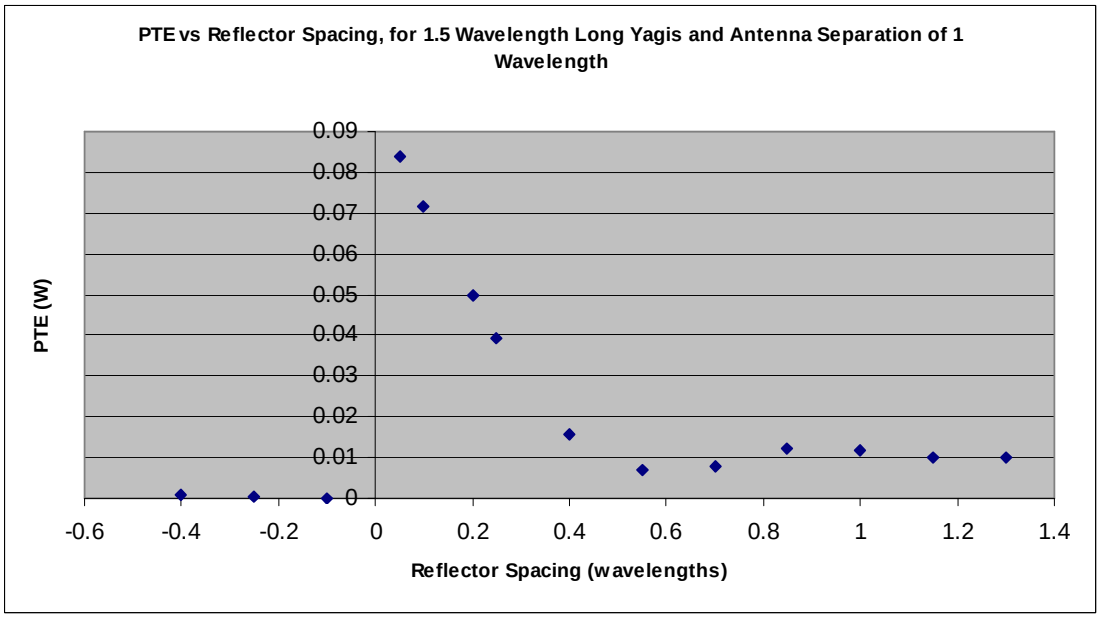

It is obvious from these results that the optimum theoretical Yagi configuration occurs when the length of all Yagi antenna elements was 0.5 wavelengths, and the reflector spacings (the symbols ‘d’ in Figure 3.3) is small.

3.3 Experimental Measurements

A physical implementation of the transmitting and receiving antennas was necessary not only to confirm the simulated and theoretical two-port model, but also because the ultimate goal of the project was to have a physical implementation of the power transfer system.

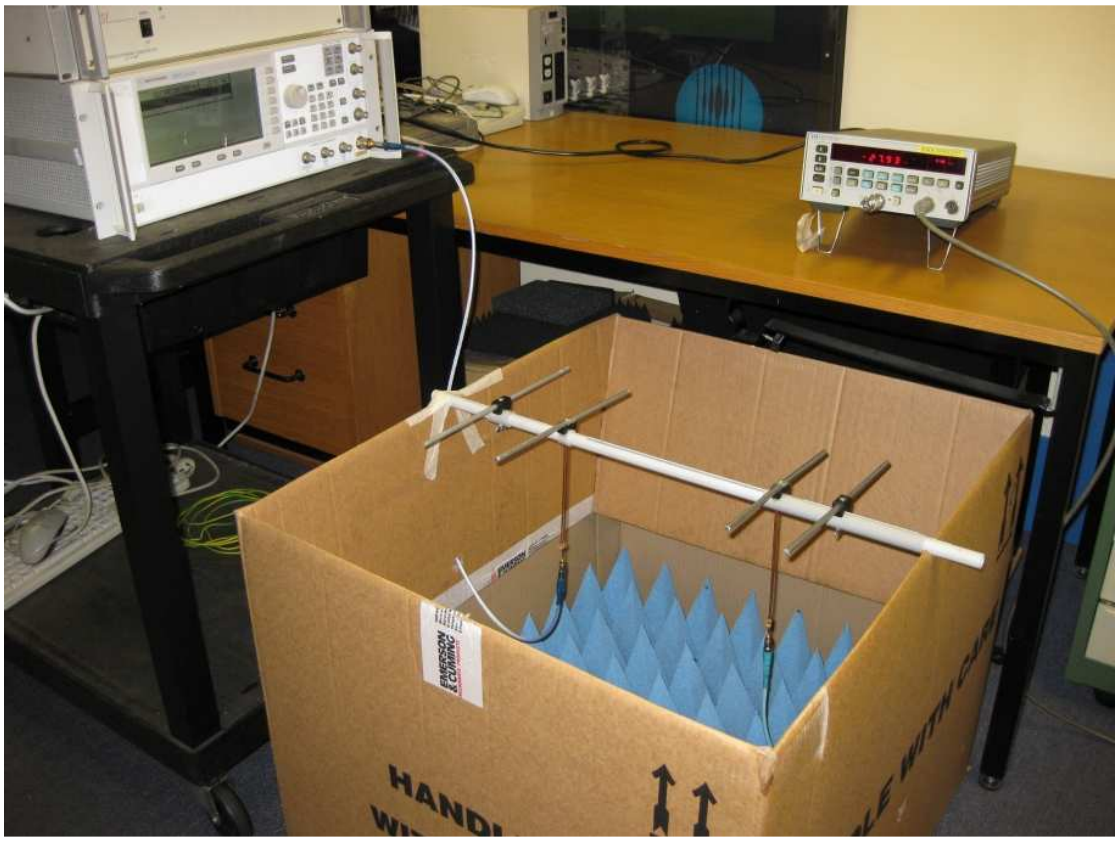

Figure 3.9: Experiment set-up for experimental measurements.

The experimental set-up is shown in Figure 3.9 above. Both Yagi antennas had a balun connected to their feedpoint, in order to balance the currents on the antennas, as well as to match the source and measuring instruments to the single driven and load elements of the two antennas. The reflector distance for both antennas, as well as the distance between both antennas, can be modified. The frequency of operation was designed to be 527MHz, and both elements for both antennas were about half-wavelength long. A power source set at -20dB was connected to the transmitting antenna feedpoint, and a power measuring instrument was connected to the feedpoint of the receiving antenna (see Figure 3.9). The measurements were carried out by choosing a configuration for the Yagi antennas (reflector spacing for both transmitting and receiving antennas) then the distance between the antennas was varied. The power at various separation distances was measured and recorded.

3.4 Comparison of Results

The Power Transfer Efficiency versus antenna separation distance was firstly calculated using the two-port network model, and compared to simulation results, as shown below.

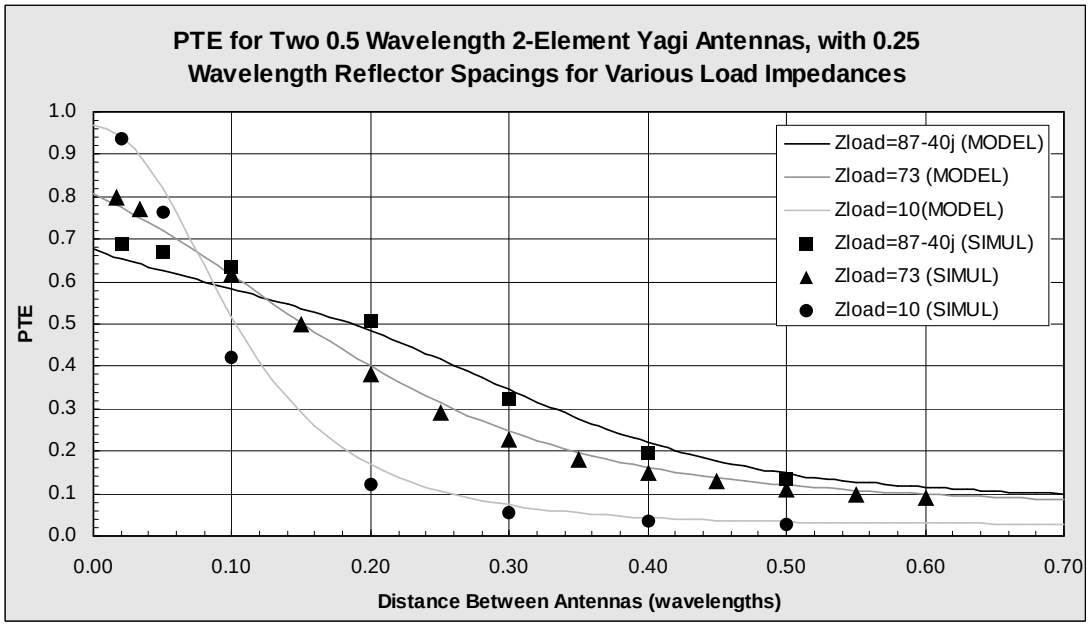

Figure 3.10: PTE for two 0.5 Wavelength 2-element Yagi antennas, with 0.25 Wavelength reflector spacings for various load impedances. Comparison between simulation and 2-port model

Figure 3.10 compares the simulated PTE results to the two-port model PTE results for two Yagi antennas both with 0.25λ reflector spacing, for various load impedances. It can be seen that the model and simulation results from nec2 exhibit the same behaviour and are very similar especially as the distance increases above about 0.1 wavelengths. It can be seen that the 10Ω load is a better match to the receiving antenna at small antenna separation, while the 87-40iΩ load is a better match to the receiving antenna at large antenna separations.

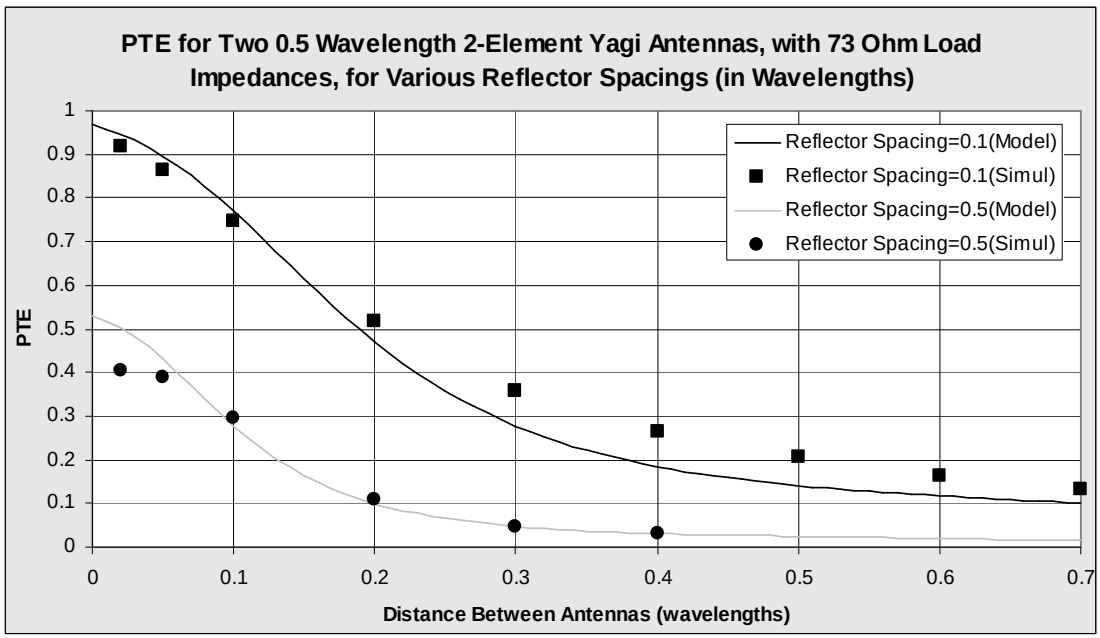

Figure 3.11 – PTE for Two 0.5 Wavelength 2-Element Yagi Antennas, with constant 73 Ohm Load, for Various Reflector Spacings (in Wavelengths). Comparison between Simulation and 2-Port Model

Figure 3.11 compares the simulated PTE results to the two-port model PTE results for two Yagi antennas with a constant 73 Ohm load on the receiving antenna, for two different reflector spacings. It can be seen that the model and simulation results exhibit the same behaviour, and similar results. Also, as expected from optimum Yagi configuration investigation of Figure 3.8, the smaller reflector spacing (0.1λ) produces greater power transfer.

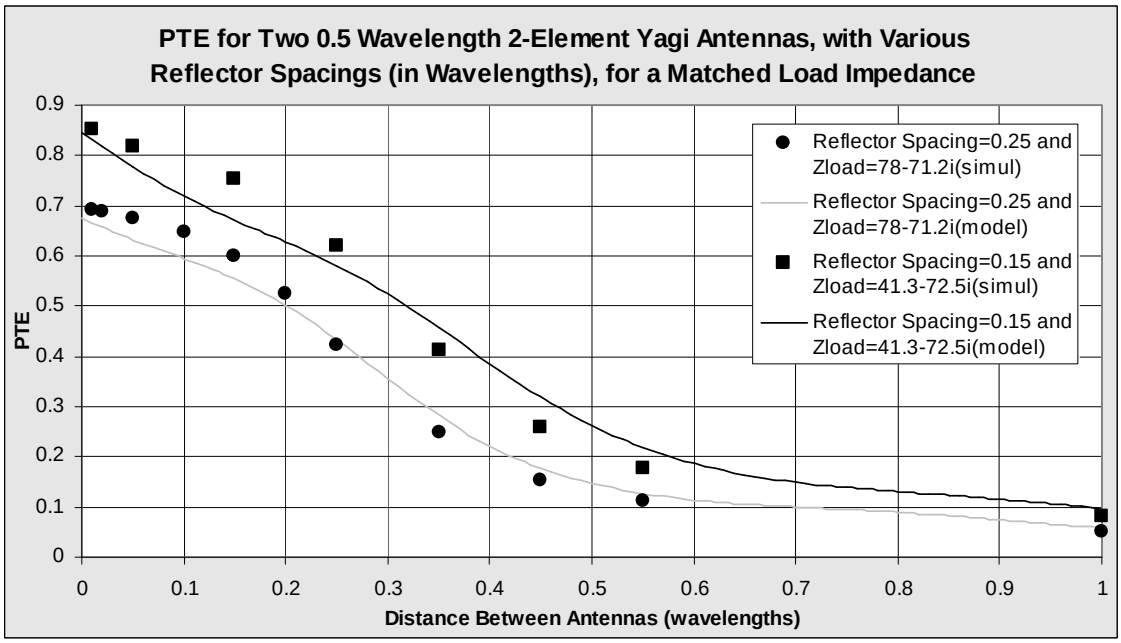

Figure 3.12 – PTE for Two 0.5 Wavelength 2-Element Yagi Antennas, with Various Reflector Spacings (in Wavelengths), and with Matched Load Impedance. Comparison between Simulation and 2-Port Model

Figure 3.12 compares the simulated PTE results to the two-port model PTE results for two Yagi antennas with a matched load on the receiving antenna, for two different reflector spacings. It can be seen that the model and simulation results exhibit the same behaviour, and similar results. Also, as expected from the optimum Yagi configuration investigation of Figure 3.8, the smaller reflector spacing (0.15λ) produces greater power transfer. In addition to this, as expected from the investigation of maximising Power Transfer Efficiency in section 3.1.4, the matched load (matched at far field distances) produces greater power transfer (at far field distances) when compared to Figure 3.11, which does not have a matched load.

The computed predictions are now compared with the experimental results in Figure 3.13. The Power Transfer Efficiency versus antenna separation distance was calculated using the two-port network model, and compared to simulations and experimental measurements in Figure 3.15.

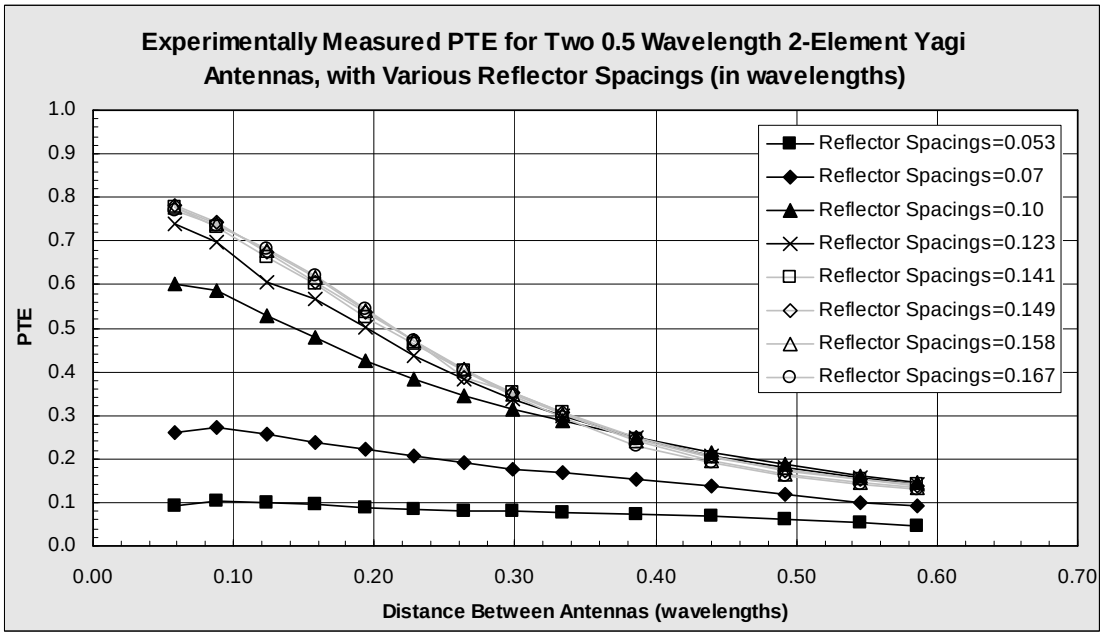

Figure 3.13: Experimentally measured PTE for two 0.5 wavelength 2-element Yagi antennas, with various reflector spacings (in wavelengths)

Looking at the experimentally measured results in Figure 3.13, it is seen that the results are not as expected from the simulation study on the optimum Yagi configuration, since it appears that power transfer is low at close reflector spacings, and peaks at a reflector spacing of about 0.15λ. It was expected that closer spacings would result in better power transfer for half-wavelength Yagi antennas, as seen in Figure 3.8. This discrepancy is likely caused by a retuning of the input impedance by the baluns, as well as the fact that the antenna elements were not exactly half-wavelength long, which would cause a best tuned reflector separation distance for maximum power transfer (as seen in the decaying sinusoids in Figure 3.8).

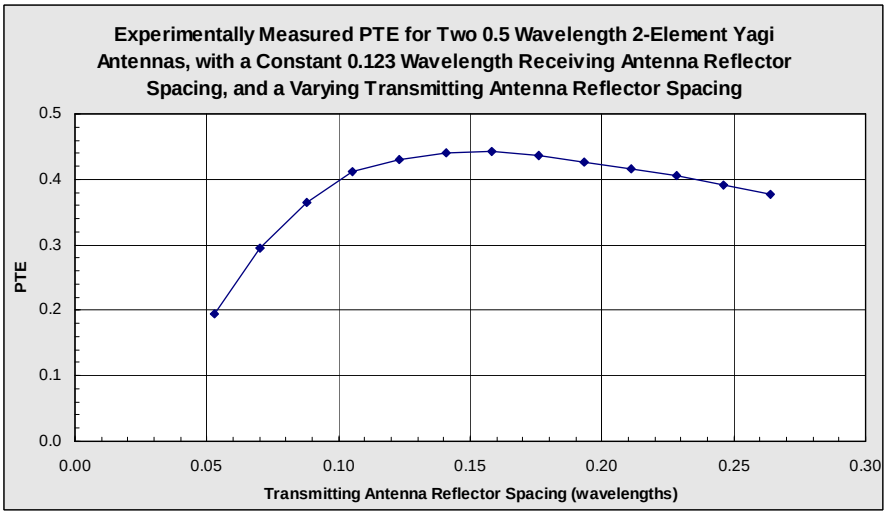

Figure 3.14: Experimentally measured PTE for two 0.5 wavelength 2-element Yagi antennas, with a constant 0.123 wavelength receiving antenna reflector spacing, and a varying transmitting antenna reflector spacing

Looking at the experimentally measured results of Figure 3.14, it can be seen that the best tuned reflector separation distance is approximately 0.15λ.

Since the antenna baluns match the instruments to the single driven and load half-wavelength Yagi antenna elements, the load impedance appearing to the load element is approximately 73-40iΩ. Simulating the 0.5λ long Yagi antennas with this load, as well as calculating the PTE with the two-port model with this load, and comparing these results to the experimental measurements for the reflectors spacing distance of 0.149λ, produces this graph (Figure 3.15).

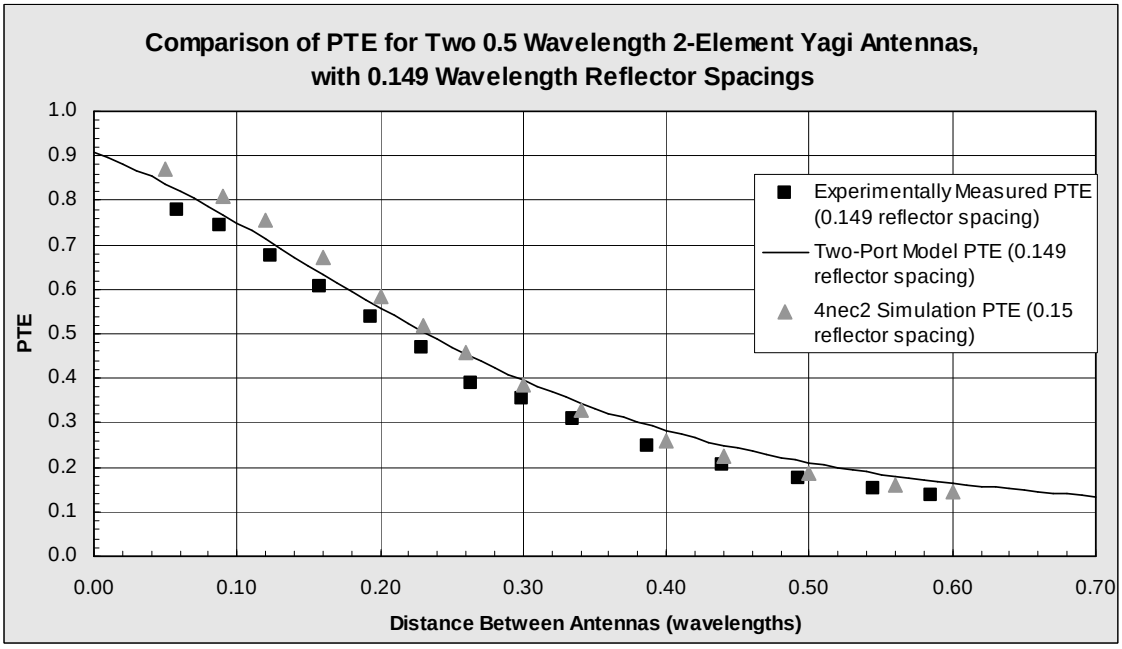

Figure 3.15: Comparison of PTE for two 0.5 wavelength 2-Element Yagi antennas, with 0.149 wavelength reflector spacings

It should be noted that the 4nec2 simulation takes into account the radius of the antenna elements, while the developed two-port network model does not. It can be seen that for this particular configuration, the experimental measurements, 4nec2 simulated measurements, and two-port network model calculations all produce fairly similar results for Power Transfer Efficiency. Thus, both the two-port network model and 4nec2 simulations provide a fairly accurate method of estimating the actual power transfer possible between two Yagi antennas.

3.5 Discussion

Study of the results, and comparisons of the two-port model to the simulations (Figures 3.10 – 3.12), shows that the two produce fairly similar results, and have the same behaviour. Thus, the two-port model is fairly accurate for close to half-wavelength long Yagi antennas, and provides a good indication of the power transfer possible using two element Yagi or dipole antennas. The discrepancies between the two results are most likely due to the simplifying assumptions used in the two-port model, such as the assumed sinusoidal current distribution along the

antennas, and the assumed thin-wire elements. The numerical integration to calculate the antenna impedances would also contribute inaccuracy to the two-port network model.

Comparing the experimental measurements to both the two-port model and the simulations (Figure 3.15), it can be seen that for a reflector spacing on both the receiving and transmitting antennas of about 0.15λ, all three results are fairly similar (note also, that for reflector spacings of 0.14λ – 0.17λ, the experimentally measured power transfer has a fairly similar behaviour, as seen in Figure 3.13). It should be noted that the relationship between power transfer and antenna separation distance, for most measured results, follow a similar curve to both the simulated and model results. However, when the reflector distance decreases to between about 0.05λ to 0.10λ, the measured results do not correspond well to either simulated or model results. As explained previously, this is likely due to the fact that the antenna elements were not exactly half-wavelength long. As well as this, when actually implementing the antennas, there are a number of issued that need to be considered, and the addressing of these issues may also have caused some discrepancies between the measurements and the two-port model and simulated results. For example, as explained previously, the antenna baluns were designed to balance the currents on the antennas, and to match the source and measuring instruments to the single half-wavelength antenna elements. Therefore, there are a few assumptions in the two-port model which may not be valid when comparing results to experimentation. In the two-port model, it is assumed that the power source is always matched to the transmitting antenna, while in experimentation, the balun matches the source instrument to the isolated single driven half-wavelength element of the Yagi antenna (not the entire Yagi antenna). Discrepancies could also be caused by reflections around the experimental antenna set-up, which would affect the measured results. The simulations and two-port models also assumed propagation in free space, which is not the case in the experimental measurements as the antennas were placed on a connecting boom (see Figure 3.9).

There are a couple of additions that can be made to the developed two-port network model. Firstly, an extension to the two-port model to include the impedance of the source as in Figure 3.16 below can be done.

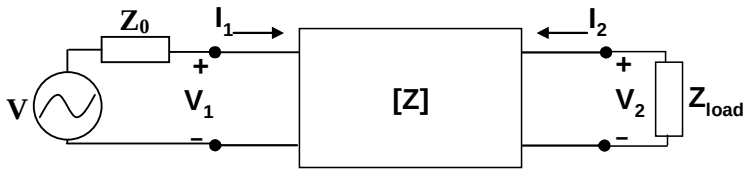

Figure 3.16: Two-port network with load and source impedance, and voltage source

This addition to the model has not been examined in depth. This model may be more useful for direct comparison with experimental work, as it uses a voltage source, as well as taking into account the impedance of the source. Secondly, the two-port model may also be extended to take into account material between the antennas, by modifying the electric field equation to consider the decay of the field through the material. This can be done in future work.

Future work should also include investigation of different antennas which may be more suitable for the application of wireless power transfer, such as smaller, integrated antennas, antennas with higher gain, and electronically tuneable antennas.

To conclude, this investigation of antennas for power transfer has provided some significant findings. The two-port network model allowed an understanding of the underlying issues surrounding antenna power transfer, as well as interesting results regarding maximum power transfer. Extensive simulations resulted in findings on the optimum configuration of the Yagi antennas, as well as confirmation of the two-port model. Finally, experimental measurements allowed study of practical considerations when implementing the antennas, as well as actual measured results. This investigation gives us an idea on the possible power transfer between two antennas.

4. RECTIFIER/VOLTAGE MULTIPLIER

After the transmitting and receiving antennas were investigated, the rectifier and voltage multiplier circuit was researched. The voltage multiplier circuit type to be examined was the Dickson Multiplier, shown in Figure 4.1 below. This circuit is used to convert the induced AC power at the receiving antenna from a lower voltage to a higher DC voltage. This circuit operates by continually switching and charging a series of capacitors, achieving an output DC voltage equal to a multiple of the input voltage magnitude, with this multiple equal to about two times the number of multiplier stages. For example, during the first AC half-cycle, the first capacitor C_1 is connected across the input voltage, charging it to the magnitude of the input AC voltage. In the next half-cycle, capacitor C_2 is connected in series with C_1 and the input AC voltage, thus charging C_2 to the magnitude of the input voltage plus the voltage already accrued on C_1, thus doubling the input voltage magnitude. This diode switching keeps continuing, ultimately producing a voltage on capacitor C_{2N} of about 2 times the number of multiplier stages multiplied by the input voltage magnitude (minus the voltage drops across the diodes). A more detailed explanation on the operation of the Dickson voltage multiplier (or charge pump) can be found in numerous articles and papers such as [9], [17] and [18]. This circuit is needed in the power transfer system, because although the power requirement of the load may be satisfied at a certain distance, the voltage need to be rectified, and may also need to be multiplied in order to meet the DC voltage requirements of the load.

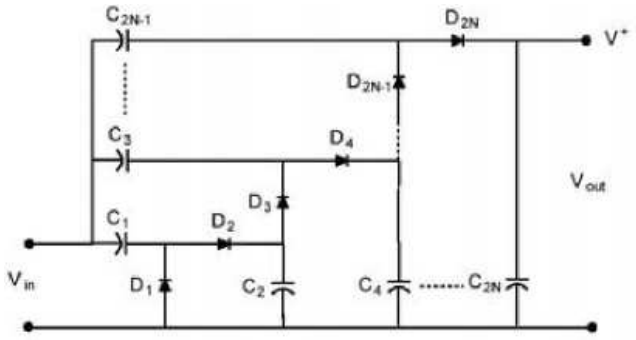

Figure 4.1: Circuit schematic of an N-stage Dickson Multiplier circuit.

An important aspect of the voltage multiplier circuit is the determination of its input impedance, in order to match the impedance of the voltage multiplier to the impedance of the receiving antenna, so as to obtain maximum power transfer to the multiplier. This determination is important, because other than the loss of power in the propagation of energy between the antennas (which the designer has little control over, other than the design of the type of antenna), any impedance mismatch between the antenna and the multiplier would be the greatest cause of power loss in the power transfer system (and the designer has control over the multiplier-antenna impedance matching) [19], [20], [21]. Finding out the input impedance of the multiplier circuit is the main focus of this chapter.

4.1 Modelling

The circuit in Figure 4.1 was simplified to obtain an estimate of the input impedance of the Dickson Multiplier. This circuit shows that if the capacitors at each stage are dimensioned to be large enough, it is possible to consider the capacitors as short circuits at the frequency of operation. As a consequence, the voltage multiplier appears to the input as a circuit of anti-parallel diodes in high frequency analysis. In the DC analysis, the capacitors can be considered as open circuits, leaving 2N diodes in series with the input, which allows the multiplication and rectification of the input voltage. Therefore the input impedance of the multiplied, Z_{mult}, is the parallel connection of 2N diodes. By replacing each of the diodes by the diode equivalent circuit of Figure 4.2 [22] [23], the input impedance of the multiplier can be modelled analytically, as derived below.

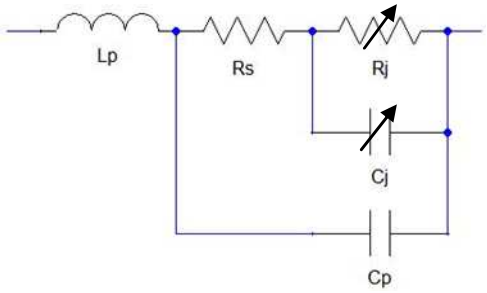

Figure 4.2: Diode equivalent circuit

$$Z_{diode} = \left\{\left[X_{Cj} \parallel R_{Rj} + R_{Rs}\right] \parallel X_{Cp}\right\} + X_{Lp} \qquad (21)$$
$$= \frac{A}{B + j\omega C_P A} + j\omega L_P$$

where $A = R_J - j\omega C_J R_J^{\,2} + R_S + R_S(\omega C_J R_J)^2$

and $B = 1 + (\omega C_J R_J)^2$

Therefore,

$$Z_{MULT} = \frac{1}{2N}\left[\frac{A}{B + j\omega C_P A} + j\omega L_P\right] \qquad (22)$$

L_P and C_P represent the diode package inductance and capacitance, respectively, R_S is the diode series resistance, while R_J and C_J are the diode junction resistance and capacitance. Unfortunately, the junction resistance and capacitance are non-linear, and are dependant on the current through the diode. Thus, a change in input power will change the junction parameters, and as a consequence, the input impedance of the multiplier. The same thing will also happen (as the current through the diode will change) when different loads are connected to the output of the multiplier circuit. Therefore, the equivalent impedance of the voltage multiplier is dependant on input power as well as output load impedance. Unfortunately, expressions for junction resistance and capacitance, depending on input power, have not been found, and so this analytical expression can only be used to very roughly estimate the input impedance of the

multiplier (by replacing the junction capacitance and resistance by their zero-bias values, which are usually provided in diode datasheets) [26].

Even though the analytical equation cannot be used for accurate design, a finding can be made from this model. Since the diodes are in anti-parallel across the input, it can be seen that an increase in the number of stages of the multiplier results in a decrease in the input impedance. As well as this, since the reactance of the diode is dominated by the junction capacitance, the multiplier has a capacitive reactance, and so an increase in the frequency of operation will cause a decrease in the input reactance. A much more thorough and in-depth analytical examination of the input impedance of the Dickson Multiplier can be found in reference [9].

4.2 Simulation

In order to obtain an accurate evaluation of the Dickson Multiplier input impedance, the input impedance can be calculated using a Harmonic Balance Simulation [24]. This simulation is performed using Ansoft Designer, using the PSPICE parameters of the HSMS-282x [25], [26] Schottky diode for the diodes in the multiplier, with the input power being swept. The circuit schematic was simply drawn up in the simulator, with an input power source, and a Harmonic Balance Analysis added for the analysis. A screenshot of the simulation set-up is shown in Figure 4.3 below.

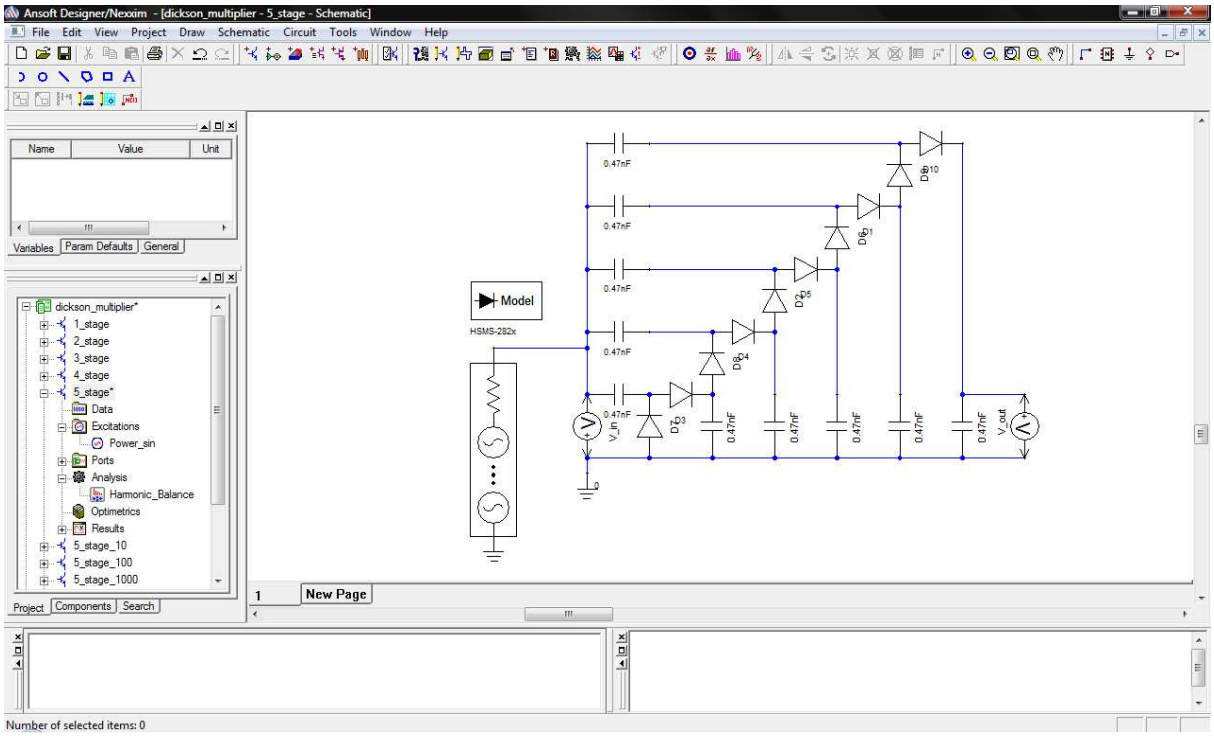

Figure 4.3: Screenshot of Harmonic Balance simulation set-up to determine input impedance of Dickson Multiplier.

4.3 Results

The input impedance simulated using the Harmonic Balance analysis, using the HSMS-282x Schottky diode, and at a frequency of operation of 527MHz, for various multiplier stage numbers, is shown in Figure 4.4 (with no load impedance across the output capacitor).

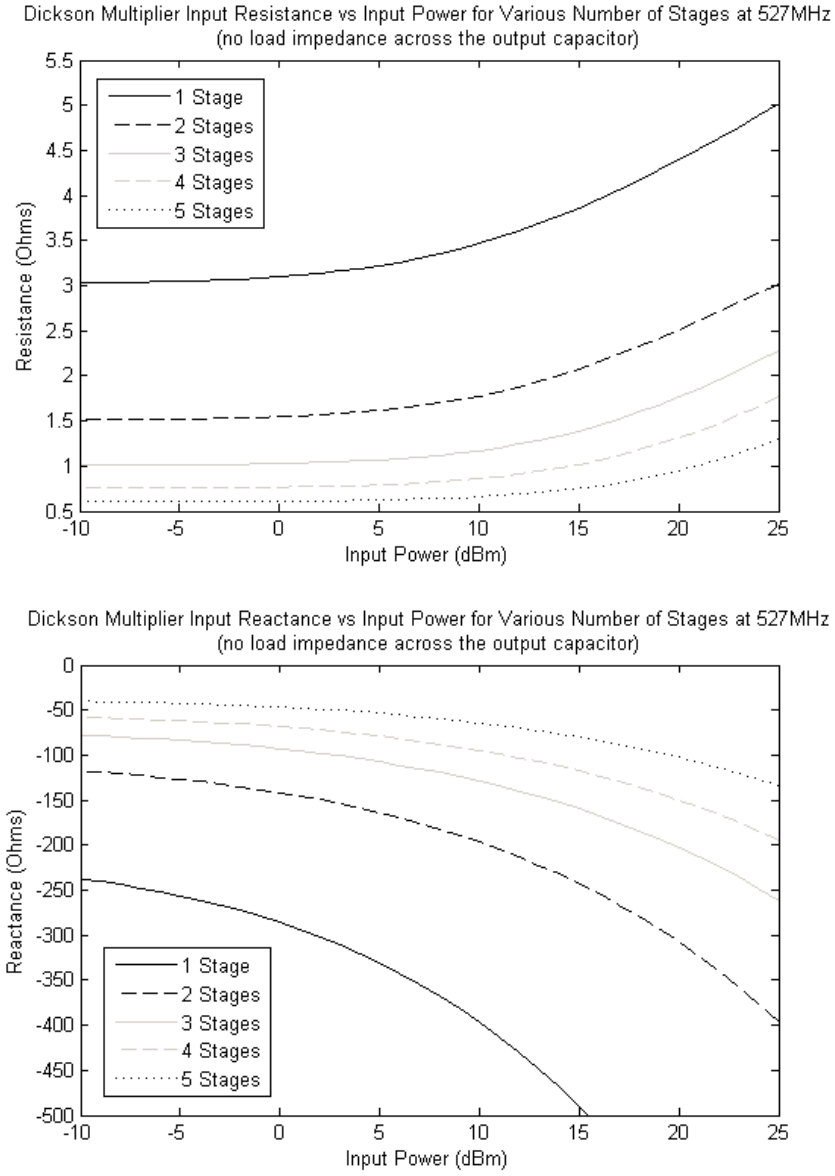

Figure 4.4: Simulated input resistance and reactance for Dickson Multiplier circuits of various number of stages and no output impedance, at 527MHz.

The input impedance simulated using the Harmonic Balance analysis, using the HSMS-282x Schottky diode, and at a frequency of operation of 527MHz, for a 5-Stage Dickson Multiplier, with various load resistances across the output capacitor, is shown in Figure 4.5.

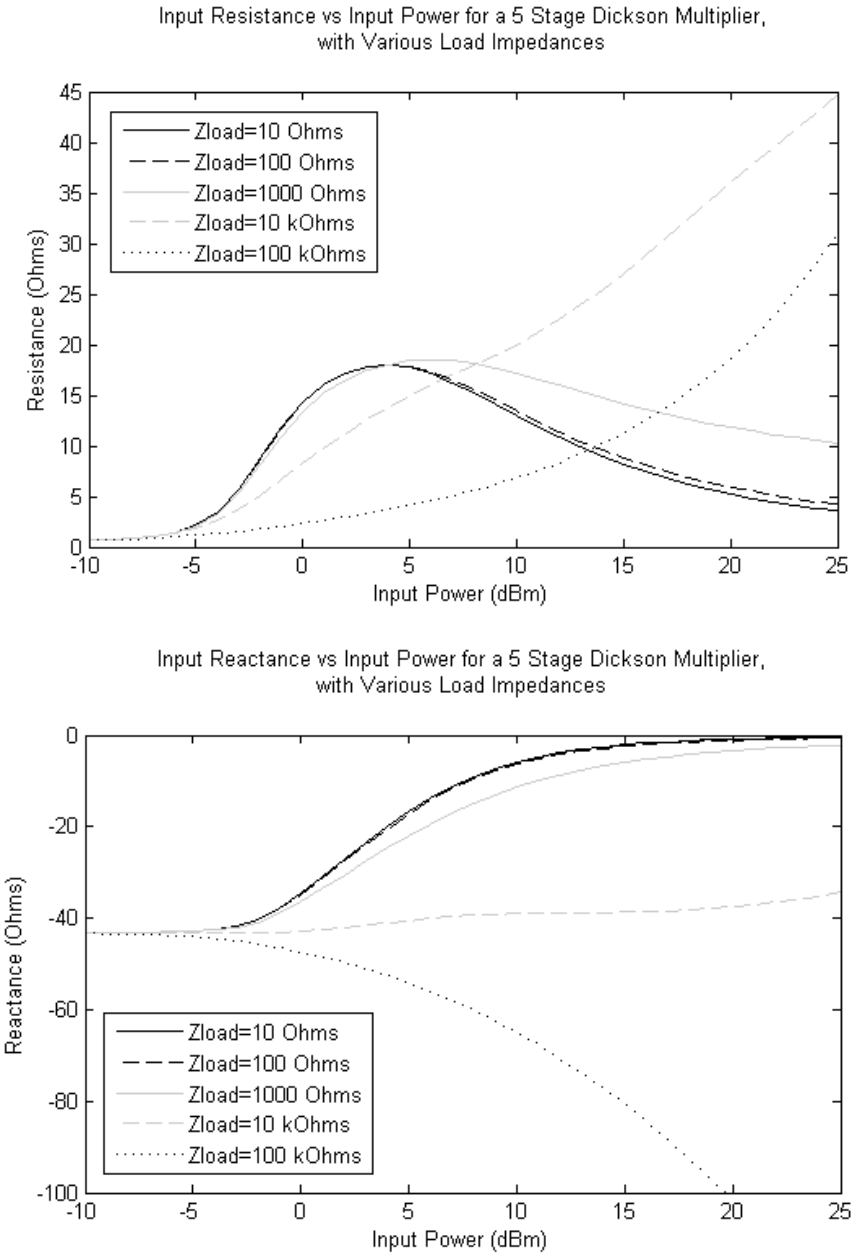

Figure 4.5: - Simulated input resistance and reactance for a 5 Stage Dickson Multiplier circuit, with load impedance across the multiplier output capacitor, at 527MHz

4.4 Discussion

Figures 4.4 and 4.5 show as expected that the Dickson Multiplier input impedance varies with input power, as well as output load impedance (as seen in Figure 4.5). As explained previously, this is due to the non-linear nature of the diodes in the multiplier circuit, so that the diode equivalent impedance changes with bias voltage and current. Figure 4.4 also shows that the multiplier input impedance decreases as the number of stages increases (i.e. doubling the number of stages results in a halving of the input impedance), since the diodes appear anti-parallel to the input source. Note that the circuits were simulated at 527MHz, since the

experimental antennas were implemented for use at this frequency, but due to lack of time, the results were not used in the production of an electronic circuit for use with the experimental antennas.

In order to design an impedance matching circuit to match the multiplier circuit to the receiving antenna, firstly, the minimum power for correct operation of the load must be determined (which is the power induced at the receiving antenna for a matched load), and then the corresponding distance for this power level must be found. Once this distance is found, the number of multiplier stages must be selected, with consideration to the voltage requirement of the load and the voltage induced at the receiving antenna at the required distance, as well as possibly obtaining an impedance of the multiplier that can be easily matched to the receiving antenna.

It should also be noted that if the impedance matching circuit is not properly designed, this would result in an impedance mismatch between the multiplier circuit and the receiving antenna, which would in turn cause a loss of input power, which would then affect the input impedance of the multiplier, which would cause a further impedance mismatch, and thus further input power loss. The overall consequence of an inaccurately designed matching circuit would be a reduction in the possible maximum distance for correct operation of the load.

5. BASIC SYSTEM

The antenna two-port model and the multiplier circuit can be used to simulate the basic power transfer system. This system and the results obtained from the model are described in this section.

5.1 Simulation

The basic power transfer system was implemented in the circuit simulation program Ansoft Designer, using the two-port equivalent T network for the transmitting and receiving antennas, a 3-stage Dickson Multiplier circuit and an LC impedance matching network to match the multiplier circuit and the receiving antenna. A screenshot of the basic power transfer system in simulation is shown in Figure 5.1 below.

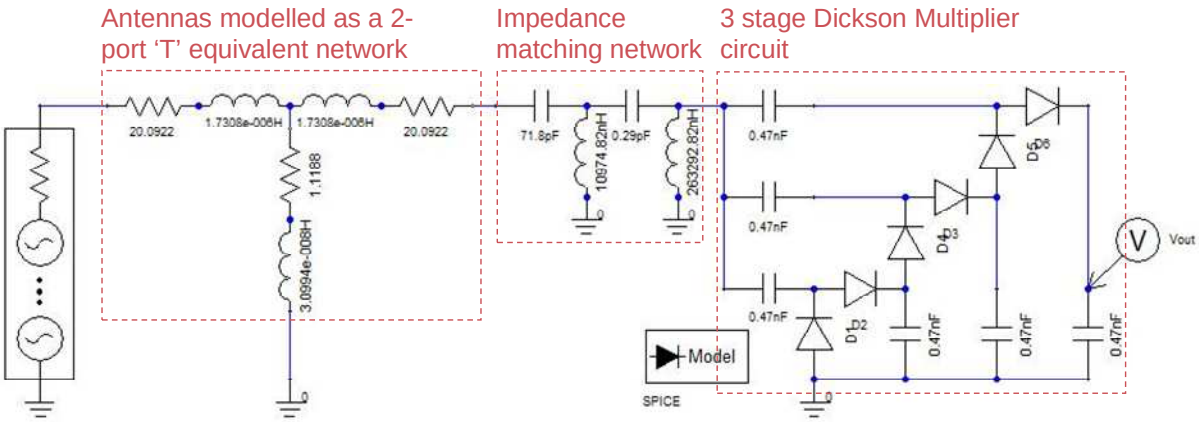

Figure 5.1: Basic power transfer system simulation circuit schematic, for an operating frequency of 5.27MHz.

A one watt power source was connected to the input, and a voltage probe was connected to the output capacitor of the multiplier circuit. A Transient Analysis was added for the analysis of the transient response of the output voltage. Unfortunately, due to large amount of time it would take to analyse the transient response of this circuit at 527MHz, the circuit had to be re-designed and simulated for a frequency of operation of 5.27MHz. Even so, the point of this exercise was to obtain a general idea on the output voltage response of the basic power transfer system, and it is assumed that the same basic design principles hold for higher frequencies. Firstly, the antennas were chosen to be half-wavelength Yagi antennas with 0.1 wavelength reflector spacings to maximize the PTE, and the impedance parameters of this antenna system were calculated using the two-port model, for a distance between the antennas of 10.4 wavelengths. The input impedance of the Dickson Multiplier at 5.27MHz was then estimated at a chosen input power level of about 0 to 1dBm. The impedance matching network was then designed to transform the input impedance of the multiplier to the conjugate impedance of the isolated receiving antenna, using standard Smith chart methods. It should also be noted that it was extremely difficult to match the impedance of the multiplier to the antenna, due to the very

large capacitive reactance of the multiplier, which was due to the low frequency of operation. This is not expected to be as big a problem at the higher frequency of operation that is intended for the actual system. Finally, the entire circuit was simulated. This calculation was then repeated. The impedance parameters of the two-port T network were modified to the impedance parameters for a distance of 9.4 wavelengths between the transmitting and receiving antennas, and then again for a variety of other distances. The output voltage transient response for these various antenna distances was recorded. Note that due to time constraints the circuit model was not well designed. For instance, the matching network was not designed in the manner discussed in section 4.4, as the simulation was done purely to get a general idea on the behaviour of the output voltage response of a basic power transfer system.

5.2 Results

The output voltage transient response of the 5.27MHz power transfer system at 1 watt input, was calculated in the manner described in the previous section, for distances between the transmitting and receiving antennas that varied between 0.4 to 10.4 wavelengths. The results are shown in Figure 5.2.

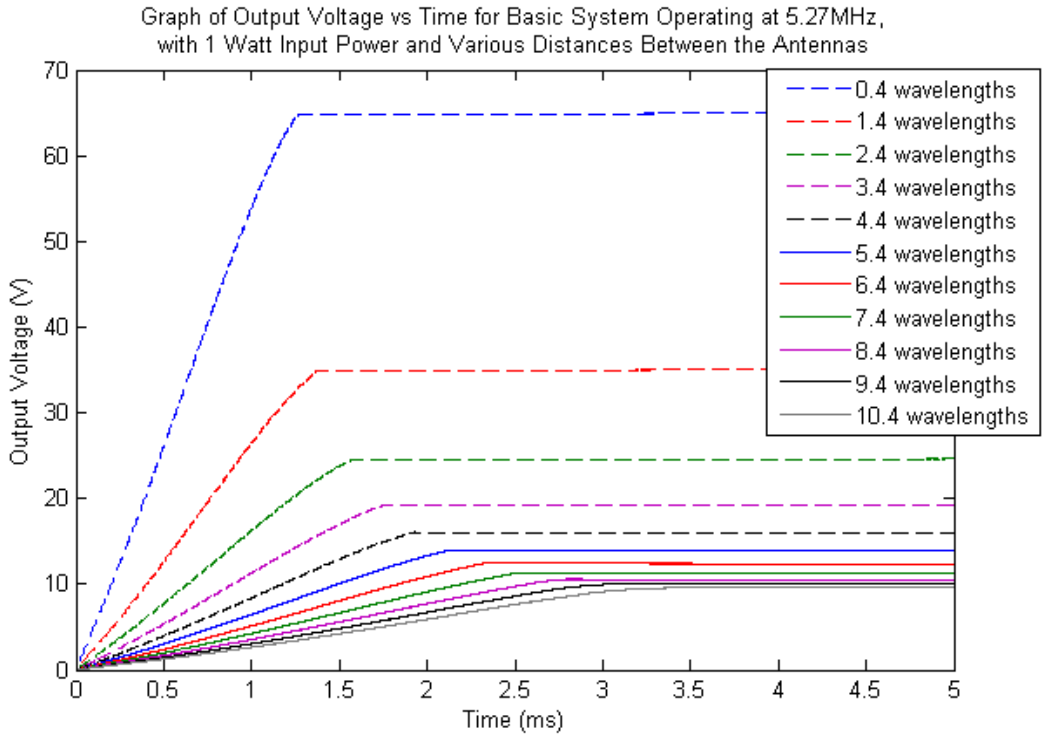

Figure 5.2: Graph of simulated output voltage versus time for basic system operating at 5.27MHz, with 1 watt input power and various antenna separation distances.

5.3 Discussion

Figure 5.2 shows that the achievable output voltage decreases as the distance between the transmitting and receiving antennas increases as one expects. If the distance is doubled the output voltage reduces by about 30%. It is interesting to note that the time taken to reach the eventual output voltage increases as the distance between antennas increases (as in Figure 5.3). This is likely due to the fact that the reduced induced voltage at greater distances means that it takes longer for the output voltage to build up, as well as the fact that maybe the voltage drop across the diodes is greater comparatively (when compared to the ultimate output voltage) at lower input voltages, and so has a greater effect at farther distances between the antennas.

Unfortunately, due to lack of time, it was not investigated whether the output voltages of Figure 5.2 corresponds well with theory. The output voltage of the Dickson multiplier can be estimated as $2N(V_{in}-V_{diode})$, where N is the number of multiplier stages, V_{in} is the magnitude of the input voltage and V_{diode} is the voltage drop across the diode. The input voltage to the multiplier of the simulated circuit should have been measured, for comparison of Figure 5.2 with this estimated equation, as well as comparison with the two-port network model.

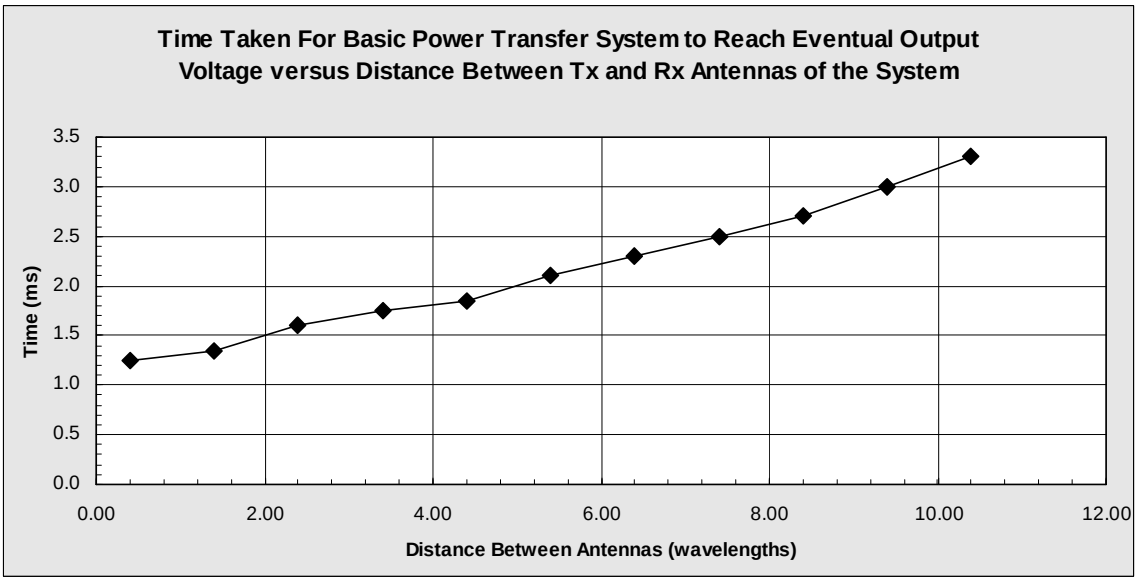

Figure 5.3: Time taken for system to reach output voltage vs distance between Tx and Rx antennas

Even though this circuit was designed at a lower frequency of operation than the intended 527MHz, it can be assumed that the circuit at 527MHz would exhibit similar behaviour, although parasitic capacitances may play a greater role at higher frequencies. It should also be noted, that at the higher frequency of 527MHz intended for implementation, the times taken to reach the eventual output voltage would be much smaller than at the 5.27MHz simulations here. It is likely that at 100 times the frequency, it would take 1/100 of the time to reach the eventual output voltage (however, this has not been examined during this investigation).

It should also be noted that the equivalent two-port T network was tested on its own, to compare the output voltage at the receiving antenna in simulation to the expected induced voltage from the Matlab model. It was found that the two had fairly similar results.

Note, also, that in an actual implementation of the multiplier circuit the actual capacitors may have a voltage limit on them, in which case the output voltage reached in simulation (Figure 5.2) would cause damage to the circuit. In this case, a low power loss voltage limiter may be implemented to make sure the voltage across the capacitors stays below a maximum level (e.g. a Zener diode voltage limiter).

This power transfer simulated circuit can also be used along with other types of antennas, since the impedance parameters for more complicated antennas can be found using NEC simulation.

In conclusion, this simulation of a basic power transfer system has provided a rough estimate of the possible behaviour of the basic power transfer system.

6. CONCLUSION/FUTURE WORK

In conclusion, this report provides a fairly comprehensive account of my research in this project of wireless power transfer. A number of interesting findings have been uncovered in this report; findings relating to the power transfer between antennas (such as the derivation of matching conditions for maximum power transfer), as well as the voltage multiplier circuit. As well as this the behaviour of a basic wireless power transfer system has been investigated in simulation. It can be argued that the design of a wireless power transfer system is complicated, with many intertwining issues relating to impedance matching needing to be considered. Simulation of the components of the system is likely to be the best method of creating a well designed wireless power transfer system.

There are still a large number of issues that need to be researched, and a number of things that need to be done in future work. First and foremost, the voltage multiplier circuit and LC impedance matching network should be designed and implemented on a PCB, for use with the already existing 527MHz Yagi antennas. This would form the basic wireless power transfer system for experimental measurements, and to obtain a direct assessment of the actual feasibility of wireless power transfer using antennas for powering low-power sensor devices. Different loads could also be connected to the multiplier circuit, such as a low-power LED for demonstration purposes.

Different antennas, which may be more suitable for actual implementation, should be researched, such as smaller, integrated antennas, antennas with greater gain and directivity, and electronically tuneable antennas for better gain-bandwidth and efficiency properties. A well selected and designed antenna that would be tuneable to obtain an impedance that is already matched to a selected multiplier circuit configuration should also be investigated, as this would remove the need for the impedance matching network.

Further investigation of the voltage multiplier circuit is also needed, in order to determine the transient charging characteristics, as well as to determine the effect of the selected diode type and capacitor values on these characteristics. Research on different multiplier circuits should also be conducted, to find out if there are better configurations.

An adaptive impedance matching network, one that adapts to changes in input power levels or output load impedance could also be researched, such as the one described in this Powercast patent [27]. It is interesting to note that Powercast, the only company to commercialize such a wireless power transfer system, have a number of patents relating to impedance matching.

Power delivery strategies and the power management circuit must also be investigated. One idea would be to use a Schmitt trigger to provide power to the load once a specified voltage level on the output capacitor is reached, which then returns to charging the capacitor once the voltage on the capacitor falls below a specified level.

The effect of a battery as a load should be researched as well, since the impedance of a battery changes as its voltage increases (i.e. the current-voltage and thus impedance of the battery is non-linear as it charges).

Finally, the ability to recharge a battery using a wireless power transfer system described in this report should be investigated.

REFERENCES

[1] S. Roundy, P. K. Wright, and J. M. Rabaey, “Energy Scavenging for Wireless Sensor Networks: with Special Focus on Vibrations,” Kluwer Academic Publishers, 2003.

[2] J. Thomas, M. Qidwai, and J. Kellogg, "Energy scavenging for small-scale unmanned systems,” *Journal of Power Sources*, vol. 159, pp. 1494-1509, 2006.

[3] G. Park, C. Farrar, M. Todd, W. Hodgkiss, and T. Rosing, “Energy Harvesting for Structural Health Monitoring Sensor Networks,” Los Alamos National Laboratory, 2007.

[4] K-Y. Lin, T. Tsang, M. Sawan, and M. El_Gamal, “Radio-Triggered Solar and RF Power Scavenging and Management for Ultra Low Power Wireless Medical Applications,” *IEEE ISCAS*, pp. 5728-5731, 2006.

[5] T. Ungan, and L. Reindl, “Harvesting Low Ambient RF-Sources for Autonomous Measurement Systems,” *IEEE International Instrumentation and Measurement Technology Conference*, 2008.

[6] H. Yan, J. Montero, A. Akhnoukh, L. de Vreede, and J. Burghartz, “An Integration Scheme for RF Power Harvesting,” 2005.

[7] T. Sogorb, J. Llario, J. Pelegri, R. Lajara, and J. Alberola, “Studying the Feasability of Energy Harvesting from Broadcast RF Station for WSN,” *IEEE International Instrumentation and Measurement Technology Conference*, 2008.

[8] D. Harrist, “Wireless Battery Recharging System Using Radio Frequency Energy Harvesting,” *Master’s Thesis*, University of Pittsburgh, 2001.

[9] G. De Vita, and G. Iannaccone, “Design Criteria for the RF Section of UHF and Microwave Passive RFID Transponders,” *IEEE Transactions on Microwave Theory and Techniques*, vol. 53, pp. 2978-2990, 2005.

[10] J-W. Lee, H. Kwon, and B. Lee, “Design Consideration of UHF RFID Tag for Increased Reading Range,” *IEEE*, 2006.

[11] N. Tran, B. Lee, and J-W. Lee, “Development of Long-Range UHF-band RFID Tag chip Using Schottky Diodes in Standard CMOS Technology,” *IEEE Radio Frequency Integrated Circuits Symposium*, pp. 281-284, 2007.

[12] T. Deyle, C. Anderson, C. Kemp, and M. Reynolds, “A foveated passive UHF RFID system for mobile manipulation,” Georgia Tech University, 2008.

[13] K. Rao, P. Nikitin, and S. Lam, “Impedance Matching Concepts in RFID Transponder Design,” *IEEE*, Intermec Technologies Corporation, 2005.

[14] C. A. Balanis, “Antenna Theory: Analysis and Design,” 3rd Ed, Wiley-InterScience, 2005.

[15] R. Olsen, “EMC Applications for Expert MININEC,” *IEEE Practical Papers, Articles and Application Notes*, available from: http://www.ieee.org/organizations/pubs/newsletters/emcs/spring03/practical.html, 2003.

[16] A. Voors, “4nec2: NEC Based Antenna Modeler and Optimizer,” *Program*, available from: http://home.ict.nl/~arivoors/, 2009.

[17] F. Bo, D. Yujie, Z. Xiaoxing, and Lu. Yingjie, “Modeling and Analysis of Power Extraction Circuits for Passive UHF RFID Applications,” *Chinese Institute of Electronics Journal of Semiconductors*, vol. 30, 2009.

[18] J. Witters, G. Groeseneken, and H. Maes, “Analysis and Modeling of On-Chip High-Voltage Generator Circuits for Use in EEPROM Circuits” *IEEE J. Solid-State Circuits*, Vol. 24, No. 5, pp. 1372-1380, 1989.

[19] C. Loo, K. Elmahgoub, F. Yang, A. Elsherbeni, D. Kajfez, A. Kishk, and T. Elsherbeni, “Chip Impedance Matching for UHF RFID Tag Antenna Design,” *Progress in Electromagnetics Research*, PIER 81, pp. 359-370, 2008.

[20] R. Morales-Ramos, D. Puente, J. Montiel-Nelsom, H. Milosiu, and R. Berenguer, “Optimal Impedance Matching in Passive UHF RFID Sensors,” *RFID Systech*, 2007.

[21] B. Jamali, D. Ranasinghe, and P. Cole, “Analysis of a UHF RFID CMOS rectifier structure and input impedance characteristics,” University of Adelaide, 2005.

[22] “Designing Detectors for RF/ID Tags,” *Application Note 1089*, Agilent Technologies, 1999.

[23] “Designing the Virtual Battery,” *Application Note 1088*, Agilent Technologies, 1999.

[24] M. Laudien, “Radio Frequency Identification (RFID) Antenna and System Design,” *Converge: An Application Workshop for High-Performance Design*, Ansoft Corporation, pp.14-15.

[25] “HSMS-282x Surface Mount RF Schottky Barrier Diodes,” *Datasheet*, Avago Technologies, pp. 3, 2008.

[26] “Linear Models for Diode Surface Mount Packages,” *Application Note 1124*, Avago Technologies, 2007.

[27] C. Greene, and D. Harrist, “Method and Apparatus for High Efficiency Rectification for Various Loads,” *US Patent 11584983*, 2006.

ACKNOWLEDGEMENTS

This work was completed when the author was employed from November 2008 till February 2009 as a Vacation Scholar in the ICT Centre. He is grateful to the CSIRO for the scholarship and the opportunity to pursue the work described here. In particular he wishes to thank his supervisor Dr Trevor Bird for his supervision, support and advice. Also thanks are due to Ken Smart for designing and constructing the practical measurement setup described in Section 3.3.

APPENDIX B – ADDITION OF TWO PARASITIC ELEMENTS

The layout for the two additional parasitic elements is as follows:

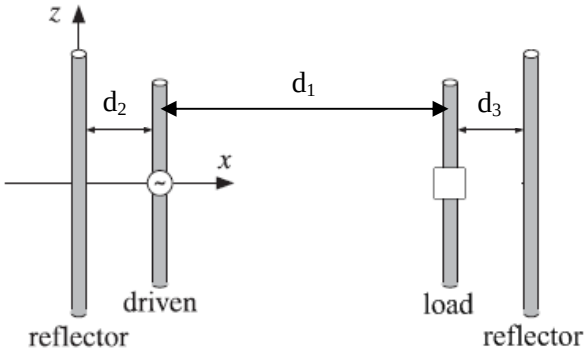

$$V_1 = Z_{11}I_1 + Z_{12}I_2 + Z_{13}I_3 + Z_{14}I_4 \qquad \text{(a)}$$
$$V_2 = Z_{21}I_1 + Z_{22}I_2 + Z_{23}I_3 + Z_{24}I_4 \qquad \text{(b)}$$
$$0 = Z_{31}I_1 + Z_{32}I_2 + Z_{33}I_3 + Z_{34}I_4$$
$$0 = Z_{41}I_1 + Z_{42}I_2 + Z_{43}I_3 + Z_{44}I_4$$

The last two equations must be solved simultaneously,

$$0 = Z_{31}I_1 + Z_{32}I_2 + Z_{33}I_3 + Z_{34}I_4 \qquad (1)$$
$$0 = Z_{41}I_1 + Z_{42}I_2 + Z_{43}I_3 + Z_{44}I_4 \qquad (2)$$

Rearranging (1) and (2),

$$I_3 = -\left\{\frac{Z_{31}I_1}{Z_{33}} + \frac{Z_{32}I_2}{Z_{33}} + \frac{Z_{34}I_4}{Z_{33}}\right\} \qquad (3)$$
$$I_4 = -\left\{\frac{Z_{41}I_1}{Z_{44}} + \frac{Z_{42}I_2}{Z_{44}} + \frac{Z_{43}I_4}{Z_{44}}\right\} \qquad (4)$$

Sub (3) into (2),

$$0 = Z_{41}I_1 + Z_{42}I_2 + Z_{44}I_4 - Z_{43}\left\{\frac{Z_{31}I_1}{Z_{33}} + \frac{Z_{32}I_2}{Z_{33}} + \frac{Z_{34}I_4}{Z_{33}}\right\}$$
$$0 = I_1\left(Z_{41} - \frac{Z_{43}Z_{31}}{Z_{33}}\right) + I_2\left(Z_{42} - \frac{Z_{43}Z_{32}}{Z_{33}}\right) + I_4\left(Z_{44} - \frac{Z_{43}Z_{34}}{Z_{33}}\right)$$

$$\therefore I_4 = \frac{1}{\left(Z_{44} - \frac{Z_{43}Z_{34}}{Z_{33}}\right)}\left\{I_1\left(\frac{Z_{43}Z_{31}}{Z_{33}} - Z_{41}\right) + I_2\left(\frac{Z_{43}Z_{32}}{Z_{33}} - Z_{42}\right)\right\} \qquad (5)$$

This gives I_4 in terms of I_1 and I_2. Sub (4) into (1),

$$0 = Z_{31}I_1 + Z_{32}I_2 + Z_{33}I_3 - Z_{34}\left\{\frac{Z_{41}I_1}{Z_{44}} + \frac{Z_{42}I_2}{Z_{44}} + \frac{Z_{43}I_4}{Z_{44}}\right\}$$

$$0 = I_1\left(Z_{31} - \frac{Z_{34}Z_{41}}{Z_{44}}\right) + I_2\left(Z_{32} - \frac{Z_{34}Z_{42}}{Z_{44}}\right) + I_3\left(Z_{33} - \frac{Z_{34}Z_{43}}{Z_{44}}\right)$$

$$\therefore I_3 = \frac{1}{\left(Z_{33} - \frac{Z_{34}Z_{43}}{Z_{44}}\right)}\left\{I_1\left(\frac{Z_{34}Z_{41}}{Z_{44}} - Z_{31}\right) + I_2\left(\frac{Z_{34}Z_{42}}{Z_{44}} - Z_{32}\right)\right\} \qquad (6)$$

This gives I_3 in terms of I_1 and I_2. (5) and (6) must be substituted into (a) and (b) to obtain Z_{11new}, Z_{12new}, Z_{21new} and Z_{22new}. For simplification, let,

$$a = Z_{44} - \frac{Z_{43}Z_{34}}{Z_{33}} \qquad d = Z_{33} - \frac{Z_{34}Z_{43}}{Z_{44}}$$

$$b = \frac{Z_{43}Z_{31}}{Z_{33}} - Z_{41} \qquad e = \frac{Z_{34}Z_{41}}{Z_{44}} - Z_{31}$$

$$c = \frac{Z_{43}Z_{32}}{Z_{33}} - Z_{42} \qquad f = \frac{Z_{34}Z_{41}}{Z_{44}} - Z_{32}$$

$$\therefore I_3 = \frac{1}{d}\{I_1 e + I_2 f\} \qquad (5)$$

$$\therefore I_4 = \frac{1}{a}\{I_1 b + I_2 c\} \qquad (6)$$

Sub (5) and (6) into (a),

$$V_1 = Z_{11}I_1 + Z_{12}I_2 + \frac{Z_{13}}{d}\{I_1 e + I_2 f\} + \frac{Z_{14}}{a}\{I_1 b + I_2 c\}$$

$$V_1 = I_1\left(Z_{11} + \frac{Z_{13}e}{d} + \frac{Z_{14}b}{a}\right) + I_2\left(Z_{12} + \frac{Z_{13}f}{d} + \frac{Z_{14}c}{a}\right)$$

$$\therefore Z_{11new} = Z_{11} + Z_{13}\frac{e}{d} + Z_{14}\frac{b}{a}$$

$$\therefore Z_{12new} = Z_{12} + Z_{13}\frac{f}{d} + Z_{14}\frac{c}{a}$$

Sub (5) and (6) into (b),

$$V_2 = Z_{21}I_1 + Z_{22}I_2 + \frac{Z_{23}}{d}\{I_1 e + I_2 f\} + \frac{Z_{24}}{a}\{I_1 b + I_2 c\}$$

$$V_2 = I_1\left(Z_{21} + \frac{Z_{23}e}{d} + \frac{Z_{24}b}{a}\right) + I_2\left(Z_{22} + \frac{Z_{23}f}{d} + \frac{Z_{24}c}{a}\right)$$

$$\therefore Z_{21new} = Z_{21} + Z_{23}\frac{e}{d} + Z_{24}\frac{b}{a}$$

$$\therefore Z_{22new} = Z_{22} + Z_{23}\frac{f}{d} + Z_{24}\frac{c}{a}$$

Finally,

$$V_1 = Z_{11new}I_1 + Z_{12new}I_2$$
$$V_2 = Z_{21new}I_1 + Z_{22new}I_2$$

Reciprocity holds (i.e. $Z_{12new}=Z_{21new}$) for certain conditions, shown below.

$$Z_{23}\frac{e}{d} = Z_{23}\left(\frac{\frac{Z_{34}Z_{41}}{Z_{44}} - Z_{31}}{Z_{33} - \frac{Z_{34}Z_{43}}{Z_{44}}}\right) = Z_{23}\left(\frac{Z_{34}Z_{41} - Z_{31}Z_{44}}{Z_{33}Z_{44} - Z_{34}Z_{43}}\right)$$

$$Z_{24}\frac{b}{a} = Z_{24}\left(\frac{\frac{Z_{43}Z_{31}}{Z_{33}} - Z_{41}}{Z_{44} - \frac{Z_{43}Z_{34}}{Z_{33}}}\right) = Z_{24}\left(\frac{Z_{43}Z_{31} - Z_{41}Z_{33}}{Z_{44}Z_{33} - Z_{43}Z_{34}}\right)$$

$$Z_{13}\frac{f}{d} = Z_{13}\left(\frac{\frac{Z_{34}Z_{42}}{Z_{44}} - Z_{32}}{Z_{33} - \frac{Z_{34}Z_{43}}{Z_{44}}}\right) = Z_{13}\left(\frac{Z_{34}Z_{42} - Z_{32}Z_{44}}{Z_{33}Z_{44} - Z_{34}Z_{43}}\right)$$

$$Z_{14}\frac{e}{d} = Z_{14}\left(\frac{\frac{Z_{43}Z_{32}}{Z_{33}} - Z_{42}}{Z_{44} - \frac{Z_{43}Z_{34}}{Z_{33}}}\right) = Z_{14}\left(\frac{Z_{43}Z_{32} - Z_{42}Z_{33}}{Z_{44}Z_{33} - Z_{43}Z_{34}}\right)$$

Looking at these equations, as well the equations for Z_{11new}, Z_{12new}, Z_{21new} and Z_{22new}, it can be seen that if, and only if $Z_{ab}=Z_{ba}$, then $Z_{12new}=Z_{21new}$, which confirms reciprocity.

APPENDIX C – MAXIMISING POWER TRANSFER EFFICIENCY

$$PTE = \frac{P_{out}}{P_{in}} = \frac{\mathrm{Re}\{Z_{load}\}}{\mathrm{Re}\{Z_{in}\}}\left|\frac{Z_{21}}{Z_{22}+Z_{load}}\right|^2 = \left(\frac{Z_{21}}{Z_{22}+Z_{load}}\right)\left(\frac{Z_{21}}{Z_{22}+Z_{load}}\right)^* \frac{R_{load}}{R_{in}}$$

$$= \frac{Z_{21}Z_{21}^*}{(Z_{22}+Z_{load})(Z_{22}+Z_{load})^*}\frac{R_{load}}{R_{in}}$$

$$= \frac{(R_{21}+jX_{21})(R_{21}-jX_{21})}{(R_{22}+R_{load}+jX_{22}+jX_{load})(R_{22}+R_{load}-jX_{22}-jX_{load})}\frac{R_{load}}{R_{in}}$$

Looking at Z_{in}:

$$Z_{in} = Z_{11} - \frac{Z_{12}Z_{21}}{Z_{22}+Z_{load}} = (R_{11}+jX_{11}) - \frac{(R_{12}+jX_{12})(R_{21}+jX_{21})}{R_{22}+jX_{22}+R_{load}+jX_{load}}$$

$$= (R_{11}+jX_{11}) - \frac{(R_{12}R_{21}-X_{12}X_{21})+j(R_{12}X_{21}+R_{21}X_{12})}{(R_{22}+R_{load})+j(X_{22}+X_{load})}$$

Multiplying this by the complex conjugate of the denominator:

$$= (R_{11}+jX_{11}) - \frac{[(R_{12}R_{21}-X_{12}X_{21})(R_{22}+R_{load})+(R_{12}X_{21}+R_{21}X_{12})(X_{22}+X_{load})]}{(R_{22}+R_{load})^2+(X_{22}+X_{load})^2}\ldots$$

$$\ldots + j\frac{[(R_{12}X_{21}+R_{21}X_{12})(R_{22}+R_{load})-(R_{12}R_{21}-X_{12}X_{21})(X_{22}+X_{load})]}{(R_{22}+R_{load})^2+(X_{22}+X_{load})^2}$$

Therefore, the real part of Z_{in} is:

$$\therefore \mathrm{Re}\{Z_{in}\} = (R_{11}R_{22}{}^2 + 2R_{11}R_{22}R_{load} + R_{11}R_{load}{}^2 + R_{11}X_{22}{}^2 + 2R_{11}X_{22}X_{load} + R_{11}X_{load}{}^2)\ldots$$
$$\ldots - [R_{12}R_{21}R_{22} + R_{12}R_{21}R_{load} - X_{12}X_{21}R_{22} - X_{12}X_{21}R_{load} + R_{12}X_{21}X_{22} + R_{12}X_{21}X_{load}\ldots$$
$$\ldots + X_{12}R_{21}X_{22} + R_{21}X_{12}X_{load}]) \div (R_{22}{}^2 + 2R_{22}R_{load} + R_{load}{}^2 + X_{22}{}^2 + 2X_{22}X_{load} + X_{load}{}^2)$$

This is equation (2).

Now, looking at the rest of the equation,

$$\frac{Z_{21}Z_{21}^*}{(Z_{22}+Z_{load})(Z_{22}+Z_{load})^*} = \frac{R_{21}{}^2 + X_{21}{}^2}{(R_{22}+R_{load})^2+(X_{22}+X_{load})^2}$$

This is equation (1)

Thus,

$$PTE = (1)\frac{R_{load}}{(2)}$$

If we let:

$$a = R_{21}{}^2 + X_{21}{}^2$$
$$b = 2R_{11}R_{22} - R_{12}R_{21} + X_{21}X_{12}$$
$$c = 2R_{11}X_{22} - R_{12}X_{21} - R_{21}X_{12}$$
$$d = e = R_{11}$$
$$f = R_{11}R_{22}{}^2 + R_{11}X_{22}{}^2 - R_{12}R_{21}R_{22} + X_{12}X_{21}R_{22} - R_{12}X_{21}X_{22} - R_{21}X_{12}X_{22}$$

Then the PTE reduces to:

$$PTE = \frac{aR_{load}}{bR_{load} + cX_{load} + dR_{load}{}^2 + eX_{load}{}^2 + f}$$

Finding the partial derivatives of this PTE with respect to load resistance and reactance gives:

$$PTE_{Rload} = \frac{a(bR_{load} + cX_{load} + dR_{load}{}^2 + eX_{load}{}^2 + f) - aR_{load}(b + 2dR_{load})}{(bR_{load} + cX_{load} + dR_{load}{}^2 + eX_{load}{}^2 + f)^2}$$
$$PTE_{Xload} = \frac{-aR_{load}(c + 2eX_{load})}{(bR_{load} + cX_{load} + dR_{load}{}^2 + eX_{load}{}^2 + f)^2}$$

These two equations form the gradient of the PTE equation. Solving both these equations (by firstly looking at the numerator of PTE_{Xload}) for zero results in:

$$PTE_{Xload} = c + 2eX_{load} = 0$$
$$\therefore X_{load} = \frac{-c}{2e}$$

Substituting this result for X_{load} back into PTE_{Rload} and then solving for zero gives:

$$PTE_{Rload} = \frac{a(bR_{load} - \frac{c^2}{2e} + dR_{load}{}^2 + e\frac{c^2}{4e^2} + f) - aR_{load}(b + 2dR_{load})}{(bR_{load} - \frac{c^2}{2e} + dR_{load}{}^2 + e\frac{c^2}{4e^2} + f)^2} \equiv 0$$
$$\therefore R_{load} = \sqrt[+]{\frac{f - \frac{c^2}{4e}}{d}}$$

For both X_{load} and R_{load}, the expressions for a, b, c, d, e and f can be substituted back into their equations, and simplified to ultimately end up with these final expressions:

$$R_{load} = \sqrt[+]{R_{22}{}^2 - R_{22}(R_{12}R_{21} - X_{12}X_{21})/R_{11} - (R_{12}X_{21} + R_{21}X_{12})^2/(4R_{11}{}^2)}$$
$$X_{load} = -X_{22} + (R_{12}X_{21} + R_{21}X_{12})/2R_{11}$$

APPENDIX A – REVIEW OF HARRIST THESIS

Page 2 – Harrist mentions antenna efficiency and impedance matching for the multiplier circuit, but never follows up or analyses these issues (not followed up in chapter 3).

Page 4 – Harrist talks about transmitting antenna to be used, but there are no specifics on antenna type, directionality, nor how he obtains his value for power emitted (6mW/m^2) (measured or calculated?).

Page 5 – 'The phones'. Description of the batteries included in the phones, but no mention of battery A-hr rating, which is required for proper determination of battery charging rate. Note he specifies a charge time of about 2 hours using supplied travel charger (with charging voltage of 3.6V and a large current output of 350mA).

Page 14 – equation 1, Cockcroft-Walton multiplier. Harrist stated equation 1 appears to be based on these assumptions, which he has not specified: The voltage outputted by an N-stage multiplier is equal to nV0, where V0 is the output voltage of a single stage (i.e. 2Vinpeak). The equivalent resistance of an N-stage multiplier is equal to nR0, where R0 is the equivalent resistance of a single stage. He then forms equation 1 using the simple voltage divider rule. The applicability of this equation to the actual performance of a voltage multiplier is in doubt, as the actual voltage output of an N-stage multiplier has been studied before, and none of these studies have derived a similar equation to that of Harrist. In addition to this, he does not specify the method by which to determine the equivalent (internal?) resistance of a single stage (i.e. how do you determine the internal or equivalent resistance of capacitors and diodes). (He appears to obtain this equation from a personal interview with Minhong Mi mentioned in the appendix).

Note also that if R0 is very small, then the equation reduces to approximately nV0, which is the expected output with no load (or the expected output with infinite load resistance).

Although the equation appears to indicate the importance of a low equivalent resistance R0, it cannot be used practically to determine the expected output voltage, unless a proper model of R0 is derived (which is not a simple task). If a very low internal resistance R0 is assumed anyway, then the point at which the voltage gain is negligible (i.e. Vout approaches a limit) will only occur at very high values of n, when the expression R0/RL becomes more significant (according to this equation). However, more importantly, the effects of capacitor leakage and characteristics of the diodes (voltage drop, etc.) will have a much greater effect on the steady-state output voltage of the voltage multiplier in reality, and would come into effect at smaller values of n in comparison to Harrist's stated equation. (see: 'Theoretical Performance of Voltage Multiplier Circuits' by Brugler, J.S or http://blazelabs.com/e-exp15.asp)

Page 15-16 – Harrist talks about a previous project that used the same voltage multiplier circuit as he does, that performed the same function as his circuit (using an antenna and multiplier to charge a battery). He also bases some of his simulations and circuitry on this project later in his thesis. However, he never provides any reference or detail on this project, a paper of it, or the method and outcomes of that project.

Page 17-19 – An explanation on the choice of receiving antenna is described here. Harrist however, does not go into a theoretical derivation of the expected energy harvested by the antenna itself (specifically the quarter wave whip), or the expected voltage induced by the antenna that will be inputted into the multiplier circuit. No mathematical formulas relating to antenna theory are presented in this thesis. Thus, there is no mention either of near-field or far-

field antenna theory (on top of the fact that Harrist never states the distance between his transmitting and receiving antennas). The characteristics (e.g. directionality/gain) of the antenna are also not mentioned (the commercial quarter-wave whip antenna he uses is not referenced).

Page 20 – Harrist states the variables of his system, but makes no mention of the distance between his transmitting and receiving antenna, an important parameter that would affect the characteristics of his system.

Page 22 – Harrist's justification for halving the capacitance for each stage is strange. He uses the capacitor equation q=CV, saying that since the voltage at each stage increases, the capacitance should decrease at an inverse rate in order to keep the same charge. However, the voltage does not double at each stage; it increases at a linear rate of 2nVinpeak. By his justification, the capacitance should decrease at the inverse of this rate, not halve at each stage. In any case, it is an interesting experiment, and is only tested in simulation.

Page 33-37 – Simulation results – Harrist states: 'The input is a power source, which is setup to model the RF source used in testing'. He does not, however, provide details on this input power source (which appears to be a sinusoidal input), nor gives any information on the peak voltage of this input, which is a vital value in determining the feasibility of the output of the voltage multiplier (i.e. the input peak voltage must be at least greater than the forward voltage of the diodes). It appears from the results of his simulation, that he uses an input voltage of between 5 and 6 volts (since Vout ~= 2nVin), which is a highly unlikely amount of voltage to be induced by an antenna. He provides no justification for this input voltage.

In addition to this, despite Harrist allegedly performing more than 30 simulations, he provides only 4 graphs to support the conclusions in his report (these graphs should at the very least be provided in an Appendix). His claims of little change to rise time due to changes in output capacitance and number of stages can only be confirmed through exhaustive replication of Harrist's simulations by the Thesis reader.

Lastly, personal replication of some of Harrist's simulations using LTSpice does not result in similar transient response behaviour of a 7-stage circuit, despite using the same values for circuit elements, frequency, and the same diode model. The rise time is very much quicker than that reported by Harrist.

Page 40 – Experimental results – Harrist states: 'equal stage capacitance was consistently higher (than varied stage capacitance) with output voltage'. This result does not match expected simulation results from page 36-37, but he does not provide any possible explanation for this discrepancy.

Table 3 lists the steady-state output voltage of the pcb experimental results. He again does not state what the input signal to his pcb is (i.e. it is unknown whether the signal is direct from a signal generator, or from an antenna harvesting RF energy, or what the form of the inputted signal is). It must be assumed that Harrist inputted a sinusoidal signal directly from a signal generator.

Harrist does not provide any graphs or data to compare the actual transient response to simulated results (arguably, this data may be important to the performance of the system as a whole).

Page 41 – Harrist states he cannot explain the sudden voltage drops in his results. As stated previously, his equation 1 arguably cannot be applied to this multiplier circuit. Previously stated references, which provide a more detailed study in the steady-state output of the multiplier circuit, may provide a better explanation for Harrist's results.

Page 41-42 – Harrist explains his system test setup using an antenna. No mention is made of the distance between his transmitting and receiving antennas, or the orientation to be used of the two antennas during testing.

Page 45 – After unsuccessful attempts to charge the phone via the phone circuitry (which I assume must contain electronics that regulate the method of the charging of the battery), Harrist directly connects the phone battery to his energy harvesting system. The appropriateness of this action is unknown. Study should have been carried out on battery charging (from a capacitor?), and proper methods of battery charging.

Page 55-56 – Prototype testing – Harrist explains that his monopole antennas produced about half as much DC voltage at the output of the multiplier circuit than the commercial antenna used in experimental testing of the multiplier circuit. He does not provide any data to support this statement. From this he also assumes that the efficiency of the monopole antennas are about half that of the commercial quarter-wave whip, but he does not describe any theory to explain this behaviour.

Finally, he somewhat strangely concludes that at a measured rate of 5-6mV per second supplied by his harvesting circuit (with quarter-wave whip), that the phone battery would charge from 3.2V to 3.9V (a difference of 0.7V) within about 2 hours. With his monopole antennas he gives a rate of 4mV per second, which he says would result in a charging time of 3 hours. He states also that a rate of 2mV per second obtained in previous research would result in a charging time of almost 6 hours. It appears he incorrectly calculates this battery charging time as follows:

0.7V ÷ 0.0055V/sec = 127 seconds ~= 2 minutes (not 2 hours).
0.7V ÷ 0.004V/sec = 175 seconds ~= 2.92 minutes (not 2.92 or 3 hours).
0.7V ÷ 0.002V/sec = 350 seconds ~= 5.83 minutes (not 5.83 or 6 hours).

I can only assume he calculates these charging times incorrectly as above, as he does not provide any additional detail on how he obtains these times. It seems he either incorrectly states the rate of charge (seconds instead of minutes), or he incorrectly calculates minutes as hours, as above. It is highly unlikely that Harrist's energy harvesting circuit would be able to charge the battery to full charge in about 2 hours, as he stated previously that it took 2 hours to charge the phone battery when the phone was directly connected to a wall socket using the supplied travel charger. In any case, it is doubtful that the charging time can be estimated by simply measuring the voltage across the battery during a finite interval, and then extrapolating the data to estimate the time, as I am unsure whether the charging of a battery is linear with time. The current supplied to the battery would be more indicative of the amount of time it would take to fully charge (as the time could then be estimated using the batteries A-hr rating). This is a very important mistake in his thesis, as the amount of time it takes to charge a battery, and the rate of this charging are important factors for the feasibility of such a harvesting system.

Unfortunately, Harrist does not provide any other detail on the charging time of his system. It would have been better if Harrist had continually monitored the battery voltage until it was fully charged, and measured the time it took to reach full charge, possibly providing a graph of battery voltage versus time.

The overall vagueness and lack of detail, along with the notable omissions detailed above, lead me to feel that Harrist's thesis does not provide a good foundation on which to base further research.

APPENDIX D – DESCRIPTION OF MATLAB CODES

mutual_imped.m – This function implements equation (10), and calculates the mutual impedance of two linear thin-wire elements or the self impedance of a single linear thin-wire element, using the Gauss-Legendre integration algorithm. All lengths are in wavelengths.

power_transfer_yagis.m – This function uses the function mutual_imped.m to calculate the power transfer between two 2-element Yagi antennas, by implementation of the equations (14) and (20). It outputs the power received at the load of the receiving Yagi antenna, given the properties (lengths, offsets, separations etc.) of all elements of both antennas.

power_transfer_yagis_graphing.m – This script simply makes use of the function power_transfer_yagis.m to loop through increasing distances between the transmitting and receiving Yagi antennas, and calculates and stores in a vector the power transfer between the two antennas for each distance. It then plots out a graph of power transfer efficiency versus distance between the transmitting and receiving Yagi antennas.

max_power_transfer_conditions.m – This script implements the equations (14) and (22) to determine the value of the load impedance for maximum power transfer, for two 2-element Yagi antennas as the transmitting and receiving antennas. It simply loops through increasing distances between the antennas, and calculates and stores in a vector the load impedance for maximum power transfer for each distance. It then plots out graphs of the load impedance for maximum power transfer versus distance between the transmitting and receiving Yagi antennas.

Contact Us
Phone: 1300 363 400
+61 3 9545 2176
Email: enquiries@csiro.au
Web: www.csiro.au

Your CSIRO

Australia is founding its future on science and innovation. Its national science agency, CSIRO, is a powerhouse of ideas, technologies and skills for building prosperity, growth, health and sustainability. It serves governments, industries, business and communities across the nation.